Received: 23 April 2021 | Revised: 21 December 2021 | Accepted: 7 January 2022

DOI: 10.1002/jnr.25026

RESEARCH ARTICLE

JOURNAL OF Neuroscience Research

Microglia form satellites with different neuronal subtypes in the adult murine central nervous system

Olga Bakina[1] | Helmut Kettenmann[1,2] | Christiane Nolte[1]

[1]Department of Cellular Neurosciences, Max-Delbrück Center for Molecular Medicine in the Helmholtz Association (MDC), Berlin, Germany

[2]Shenzhen Institute of Advanced Technology, Chinese Academy of Sciences, Shenzhen, China

Correspondence
Christiane Nolte, Department of Cellular Neurosciences, Max-Delbrück Center for Molecular Medicine in the Helmholtz Association (MDC), Berlin, 13092, Germany.
Email: cnolte@mdc-berlin.de

Funding information
MAX-DELBRUCK-CENTRUM FUR MOLEKULARE MEDIZIN IN DER HELMHOLTZ-GEMEINSCHAFT
Open Access funding enabled and organized by Projekt DEAL.

Abstract

Microglia are the innate immune cells of the central nervous system (CNS). In the adult uncompromised CNS, they have a highly ramified morphology and continuously extend and retract their processes. A subpopulation of microglial cells forms close soma-to-soma contacts with neurons and have been termed satellite microglia, yet the role of such interaction is largely unknown. Here, we analyzed the distribution of satellite microglia in different areas of the CNS of adult male mice applying transgenic- and immunolabeling of neuronal subtypes and microglia followed by three-dimensional imaging analysis. We quantified satellite microglia associated with GABAergic and glutamatergic neurons in the somatosensory cortex, striatum, and thalamus; with dopaminergic and serotonergic neurons in the basal forebrain and raphe nucleus, respectively; and with cerebellar Purkinje cell neurons. Satellite microglia in the retina were assessed qualitatively. Microglia form satellites with all neuronal subtypes studied, whereas a preference for a specific neuron subtype was not found. The occurrence and frequency of satellite microglia is determined by the histo-architectural organization of the brain area and the densities of neuronal somata therein.

KEYWORDS
dopaminergic, GABAergic, glutamatergic, image analysis, neuron–glia interactions, RRID:AB_1002036, RRID:AB_11205760, RRID:AB_839504, RRID:AB_90755, RRID:IMSR_JAX:007914, RRID:IMSR_JAX:014555, RRID:IMSR_JAX:016962, RRID:IMSR_JAX:016963, RRID:MGI_3052341, RRID:SCR_003070, RRID:SCR_007370, RRID:SCR_015825, satellite microglia, serotonergic

1 | INTRODUCTION

Microglia are the resident immune cells of the central nervous system (CNS) and function as a first line of defense against pathogens, during brain perturbations and in neurodegeneration. They also have important roles during development and for homeostasis in the uncompromised CNS, where they contribute to synaptic plasticity and neuronal function (Colonna & Butovsky, 2017; Kettenmann et al., 2011; Schafer et al., 2012; Tremblay et al., 2011). Microglia originate from the yolk sac and colonize the CNS during early embryonic development. In the mature healthy brain, they are characterized by a distinct ramified morphology with small cell bodies and branched processes that constantly surveil their surrounding environment (Davalos et al., 2005; Kettenmann et al., 2011; Nimmerjahn et al. 2005). Each microglial cell occupies a defined territory and microglial cell bodies are not in direct contact with each other (Lawson et al., 1990). It is well established that microglia represent a phenotypic diversity in terms of number, morphology, activity, and transcriptomics across brain regions in the adult healthy brain (De

Edited by Cristina Antonella Ghiani and Stephen J. Crocker. Reviewed by Matthew Rasband

Biase et al., 2017; Grabert et al., 2016; Masuda et al., 2020). Microglia are equipped with a plethora of neurotransmitter and neuromodulator receptors (Kettenmann et al., 2011; Pocock & Kettenmann, 2007), by which they potentially can sense synaptic activity. It has also become evident that microglia are heterogeneous with respect to their sensitivity to neurotransmitters/neurohormones (Pannell et al., 2014).

Already more than a century ago, del Rio Hortega described a subpopulation of microglia in the rabbit brain, whose cell bodies are in close contact with a neuron soma. He termed these cells satellite microglia (Del Rio Hortega, 1919). Due to their close soma-to-soma interaction they were suggested to provide trophic or metabolic support to highly active neurons (Streit, 2005). It is unknown whether the perineuronal satellite microglia plays a functional role for its partner neuron that distinguishes it from the parenchymal non-satellite microglia. In a previous study, we analyzed if an electrical cross talk exists between these closely interacting cells by simultaneous electrophysiological recordings from neurons and their satellite microglia. Although we did not find correlated neuronal and microglial activity or dye-coupling, we could identify intrinsic, spontaneous microglial activity, which was, however, also seen in parenchymal microglia.

Recently, Baalman et al. (2015) described a subpopulation of satellite microglia in the cortex called AXIS microglia. Their cell bodies are preferentially attached to the side of cortical neurons where the axon originates. AXIS microglia can form a single cellular process overlapping with the axon initial segment (AIS). This interaction depends on an intact neuronal Ankyrin G cytoskeletal scaffold. AXIS microglia occur early postnatally and reach a steady state in adult animals. Upon activation by traumatic brain injury, the contacts between microglia and AIS are reduced, suggesting that the AXIS microglia may be important for intact brain function. AXIS microglia were more often found at non-GABAergic neurons than GABAergic neurons, and more frequently associated with pyramidal neurons in cortical layer V than with the entire cortical neuron population. Although these findings indicate that direct interaction of microglia may be specific to functional subtypes of neurons and particular brain regions, the factors which determine satellite microglia formation throughout the CNS remain largely unknown.

Here, we studied the interactions of satellite microglia with different functional subtypes of neurons in the adult CNS, and assessed whether a systematic pattern exists that may be governed by tissue architectural cues in a given brain region. Transgenic reporter mice with fluorescently labeled GABAergic, glutamatergic, and serotonergic neurons and a combined immunofluorescence approach were used to label specific neuronal subtypes and the microglia population. Stacks of confocal images from different CNS regions were subjected to quantitative approaches to determine absolute neuron and microglia densities, and percentage of satellite microglia. We investigated satellite formation with GABAergic or glutamatergic neurons in the cortex, striatum, and thalamus; with the cerebellar Purkinje cells; and with serotonergic neurons in the raphe nucleus and dopaminergic neurons in the substantia nigra (SN). Our findings indicate that in the adult brain the neuronal density in a given brain region correlates with the frequency of satellite microglia. We did not find a preference for defined neuronal subtypes but found that satellite microglia are associated with all the neuronal subtypes which have been analyzed.

Significance

Microglia are the immune cells of the central nervous system. A subpopulation, satellite microglia, form direct contact of their cell body to a neuron soma. This particular neuron–glia interaction may have implications for neuron function. To understand what factors determine satellite microglia formation, we performed a morphological analysis of adult mouse brains and retinae and studied interactions with different neuronal subtypes. Satellite microglia occur in all areas containing neuron somata. Their frequency is determined by the neuron density in a given brain region, whereas a preference to form a satellite with neurons of a specific neurotransmitter subtype was not found.

2 | MATERIALS AND METHODS

2.1 | Mice

All mice used in this study were based on a C57BL/6 background, if not stated otherwise. Animals were kept according to the German law for animal protection under a 12-hr dark–light cycle with food and water supply ad libitum. Male animals aged 9–12 weeks were used for this study. The Csf1R-EGFP ("MacGreen EGFP") mouse line (RRID:MGI_3052341) expresses enhanced green fluorescent protein (EGFP), driven under the *Csf1r* (colony-stimulating factor 1 receptor) promoter in microglia (Sasmono et al., 2003). These mice were crossbred to the B6.Cg-Gt(ROSA)26Sor$^{tm14(CAG-tdTomato)Hze}$/J mouse strain (Jackson Laboratory) (RRID:IMSR_JAX:007914) with a *loxP*-flanked STOP cassette of the red fluorescent protein variant of tdTomato (Madisen et al., 2010). The resulting MacGreen EGFP × tdTomato strain was either crossbred to vglut2 (vesicular glutamate transporter2)-ires-cre knock-in mice (*Slc17a6*$^{tm2[cre]Lowl}$/J; Jackson Lab; RRID:IMSR_JAX:016963) that have Cre recombinase expression directed to excitatory glutamatergic neurons, or to vgat (vesicular GABA transporter)-ires-cre knock-in mice (*Slc32a1*$^{tm2[cre]Lowl}$/J; Jackson lab; RRID:IMSR_JAX:016962) that have Cre recombinase expression directed to inhibitory GABAergic neurons. Offspring showed Macgreen EGFP expression in microglia and robust expression of tdTomato in either excitatory glutamatergic neurons or in inhibitory GABAergic neurons. For the sake of simplicity, they are termed vgat- or vglut mice in the following. The *TPH2-ChR2(H134R)-EYFP* transgenic mice (RRID:IMSR_JAX:014555) (Zhao et al., 2011) express Channelrhodopsin-2-EYFP (enhanced yellow fluorescent protein) under the control of the promoter for tryptophan hydroxylase 2 (TPH2) which results in fluorescent labeling specific to serotonergic neurons. Mice were kindly provided by PD Dr. Friederike Klempin (Max Delbrück Center for Molecular Medicine, Berlin, Germany).

2.2 | Immunohistochemistry

Immunohistochemistry was performed on slices prepared from frozen brains or retinae and on retinal whole mounts. Mice were anesthetized (Narcorene, 100 mg/kg, i.p., Merial GmbH, Germany) and perfused transcardially with 10 ml of 0.9% saline solution followed by 50 ml of 4% paraformaldehyde in 0.1 M PB (pH 7.4). The dissected brains or eyes were postfixed in 4% paraformaldehyde in 0.1 M PB buffer for 12 h at 4 °C, then cryoprotected in sucrose (20% and 30% for 24 h each) in PBS (pH 7.4) at 4 °C, frozen in 2-methylbutane precooled on dry ice, and stored at −80°C. Frozen brains were sectioned coronally into 50-μm thick slices on a sliding microtome (Leica SM2000R, Nussloch, Germany). Brain regions were localized with the help of the *Mouse Brain in stereotactic coordinates* atlas (Paxinos & Franklin, 2001).

To isolate the retinae, the eyes were enucleated after perfusion, either postfixed and cryoprotected as above, embedded in methylcellulose and frozen. Twenty-micrometer thick transverse cryosections of the retinae were mounted to glass slides (Superfrost®Plus, Menzel-Glaser, Braunschweig, Germany).

Rabbit anti-Iba1 (1:500; FUJIFILM Wako Shibayagi cat# 019-19741, RRID:AB_839504) and chicken polyclonal anti-NeuN antibodies (1:500, EMD Merck Millipore, Darmstadt, Germany, cat# ABN91, RRID:AB_11205760) were used to label microglia and neurons, respectively. Dopaminergic neurons were labeled by sheep anti-Tyrosine Hydroxylase polyclonal antibodies (1:1,000; AB1542 Merck Millipore, Darmstadt, Germany; RRID:AB_90755). Goat polyclonal anti-green fluorescent protein (GFP) antibodies (1125; Acris Antibodies, Cat# R1091P, RRID:AB_1002036) were used to enhance the signal in serotonergic reporter mice (see Table S1). GABAergic, glutamatergic, and serotonergic neurons were identified by their transgenic labels. Primary antibodies were visualized by donkey secondary antibodies conjugted to Alexa fluor-488, Cy 3 or Alexa fluor-647 (1:200 Jackson/Dianova, Hamburg).

Immunolabeling was performed on free-floating brain slices or retinal whole mounts, and on mounted retina sections. First, slices/slides were rinsed with TBS (50 mM Tris, 146 mM NaCl, pH 7.4) and then were incubated for 15 min in a detergent-containing solution (2% Triton X-100 in TBS) followed by incubation in blocking solution (5% BSA, 5% donkey serum, 0.2% Triton X-100 in TBS) for 1 hour at room temperature. Slices were incubated with primary antibodies, diluted in 50% blocking solution for 48 hr at 4°C with gentle agitation. After several washes with TBS-T (TBS, 0.5% Tween, 0.1% BSA), slices were incubated with secondary antibodies for 2 hr at RT. Nuclei were labeled with DAPI (200 nM, in TBS). Immunolabeled slices were mounted onto glass microscope slides, embedded in Aqua Polymount media (Polysciences Europe GmbH, Germany), and kept at 4°C until image acquisition.

2.3 | Imaging

Confocal images were taken at a resolution of 1,024 × 1,024 pixels from the different brain areas (see Table S2) using an LSM700 confocal laser scanning microscope (Carl Zeiss, Jena, Germany), equipped with motorized table, four diode lasers, and controlled by Zen2010 software. *Z*-stacks with 1-μm steps were acquired from the bottom to the top optical section showing fluorescent profiles, using a Plan Apochromat 20×/NA 0.8 or a Plan-Neofluar 40×/NA 1.30 oil-immersion objective. Pinhole size was set to 1 Airy unit. For comparative analysis of the cortex, striatum, and thalamus (Figure 2), three (cortex: four) slices were scanned per animal (from three animals). For analysis of the SN, a total of nine sections (from three animals) were scanned. A total of eight sections, containing the raphe nucleus (from five animals), were scanned, and cerebellar Purkinje cells were analyzed in 15 sections from three animals. Although all slices were sectioned at a thickness of 50 μm, this thickness was not reproduced when imaging *Z*-stacks. The *Z*-stack optical thickness varied between 18 and 45 μm (27.5 ± 6.8 μm *SD*, $n = 24$ slices), which was on average 55% of the original thickness. Thickness appeared to decrease depending on the time after embedding which indicated that the slices undergo some flattening. Bermejo et al. (2003) have quantified the shrinkage of sections and reported a mean shrinkage in the *Z*-direction of 43%, which concurs with our observation. For calculating 3D volumes, we inferred the original slice thickness of 50 μm.

2.4 | 3D analysis of cell densities and microglia–neuron surface contacts

The 3D Imaris interactive software package (version 9.2, Bitplane, Oxford Instruments, RRID:SCR_007370) equipped with the colocalization tool was used to analyze the fluorescent tiled *Z*-stack images of cortical, thalamic, and striatal areas. First, four to six rectangular clippings of the *Z*-stacks were randomly selected from each brain area of interest for subsequent analysis. Surface rendering was performed on the cropped volumes for the Iba-1 channel to dissect the microglia cell body surfaces, and for NeuN or vgat td Tomato fluorescent channel to dissect the neuron soma surfaces. In case of high background fluorescence of the tdTomato signals in layer IV of the cortex, the vglut-positive neurons were first dissected with the help of fluorescence colocalization with the NeuN channel, and subsequently neuronal surfaces were rendered from the colocalization channel. In ROIs of high neuron density, touching objects were split through classifying seed points by quality. Finally, objects were filtered by number of voxels to gain only the somata. The densities of a particular cell type per ROI were determined for a given fluorescent channel. Subsequently, the Imaris surface tool (surface-to-surface contacts) was used to identify and quantify those areas where the rendered microglial and neuronal surfaces were in contact; the resulting objects were filtered for contact areas larger than 50 μm^2 (Figure 1) (see also [Wogram et al., 2016]). Colocalized contact areas of rendered surfaces were then verified manually in orthogonal view to confirm the presence of microglia to neuron soma contacts. In cases where microglia had contact to more than one adjacent neuron, multiple contact sites were merged into a single contact. Algorithms for object segmentation are given in the supplement (S2).

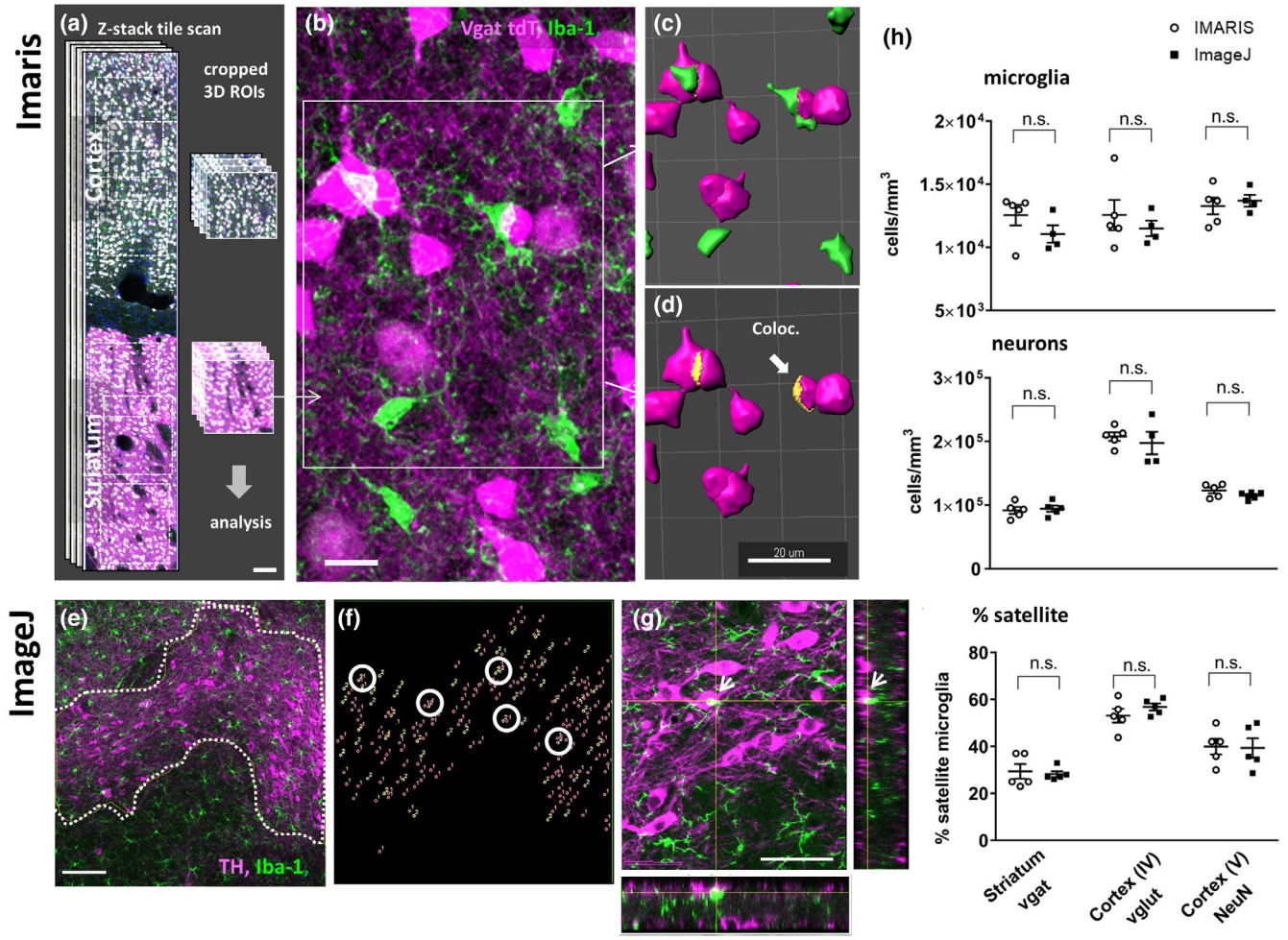

FIGURE 1 Quantitative assessment of microglia and neuronal cell densities and formation of satellite microglia in 3D volumes. (a) Imaris surface rendering approach to quantify cell densities and satellite microglia formation in rectangular volumes of interest (ROIs). *Z*-stack of confocal tile scans spanning from the cortex to striatum were obtained from immunolabeled brain sections; NeuN staining (white), vgat tdT transgenic label (magenta), and Iba-1 staining (green). From the areas of interest, *Z*-stacks of defined x–y dimension were randomly cropped (as indicated by dotted lines) for further analysis (right). (b) Confocal (projection) image from the striatum shows vgat-labeled neuronal somata (magenta) and Iba-1 immunolabeling in microglia (green), fluorescence overlap (white) indicates microglia cell bodies in contact with neuron soma. (c) 3D surface rendering image of framed area in b for vgat neurons and microglia cell bodies. (d) Same 3D volume as in d; contact areas (yellow, arrows) between microglia surfaces (masked) and vgat neuron surfaces (magenta) identified by the surface colocalization function. (e–g) ImageJ-based approach to obtain quantitative data on microglia and specific neuron densities in irregular volumes of interest (here confocal projection image of substantia nigra showing Iba-1-labeled microglia (green) and TH staining on dopaminergic neurons (magenta)). Dotted line marks ROI selected for cell counter analysis. (f) cell counter window: Microglia and TH neurons within selected ROI are marked and counted by ImageJ cell counter plugin. White circles indicate microglia closely neighboring a neuron. (g) Verification of close neighbors as satellites by orthogonal view. The flanking images on the right and below are orthogonal views. Bars indicate 100 μm in a, 10 μm in b, 20 μm in c and d, 100 μm in e, and 50 μm in g. (h) Scatterplots (mean ± *SEM*) comparing microglia densities (top), vgat-, vglut-, or NeuN- neuron densities (middle) and % satellite microglia (bottom) obtained by either Imaris and ImageJ approach in five ROIs from the striatum, somatosensory cortex layers IV and V as indicated. Pairwise comparisons of mean values obtained by ImageJ versus Imaris with two-tailed *t* test show no significant (n.s., $p > 0.05$) differences for cell densities obtained by the two quantitative approaches

To analyze cell densities in irregular shaped volumes of the deep midbrain nuclei (SN) and raphe nuclei or cerebellum, we used the ImageJ software (RRID:SCR_003070) and the Biovoxxel toolbox (RRID:SCR_015825). To determine the volume of interest in a given *Z*-stack, the area containing labeled neuronal somata was outlined with the freehand selection tool (in a Max projection image) and area size in the x–y plane was measured. The x–y area selection was copied to the *Z*-stack and the outside area cropped (see Figure 1). Subsequently, the cell counter plugin was used to determine the densities of each cell type in the different fluorescent channels throughout the cropped *Z*-stacks. Where a microglial cell was detected in the close vicinity of a neuron, the orthogonal view was used to verify direct microglia to neuron–soma contact (Figure 1). As in the Imaris approach, the

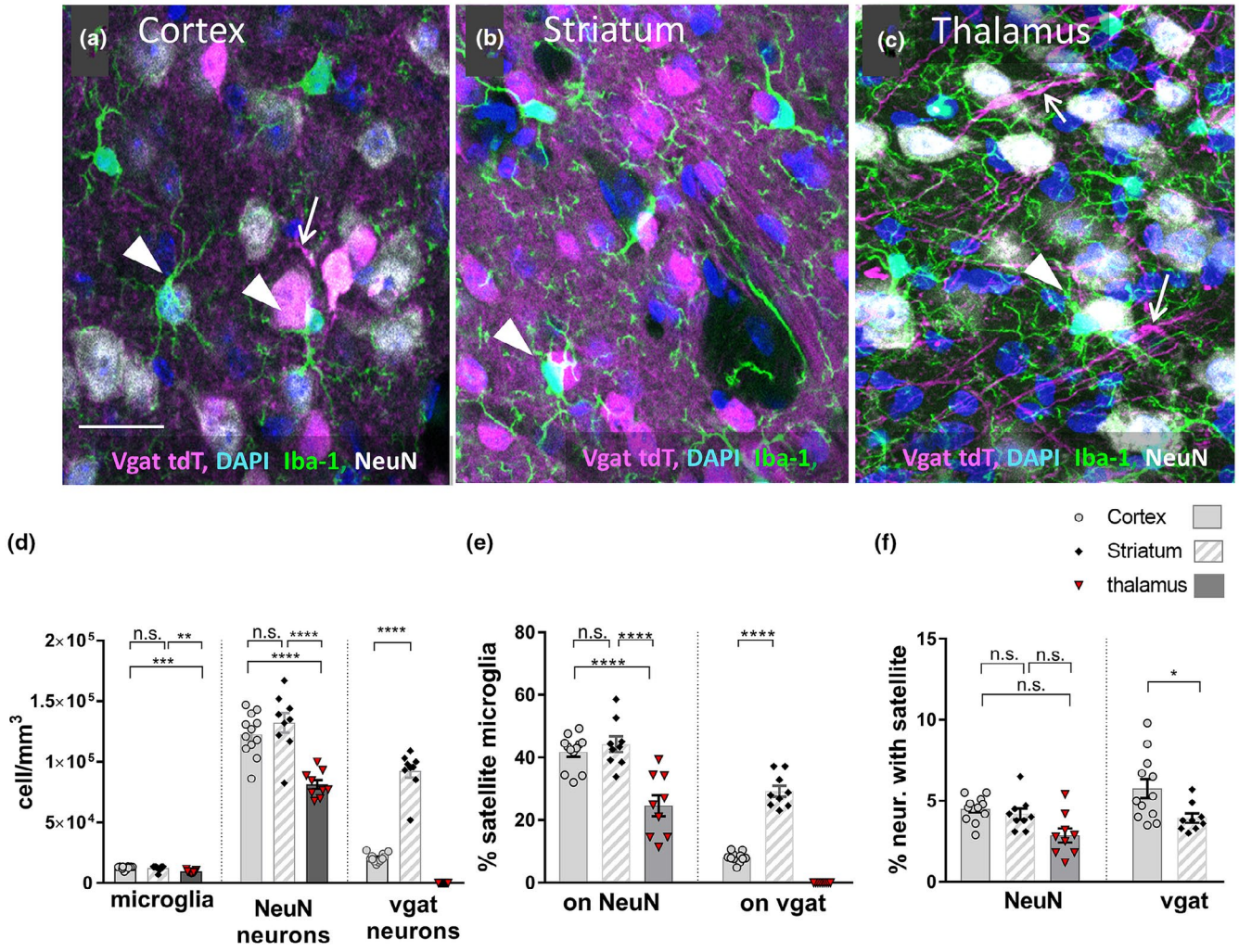

FIGURE 2 Quantitative analysis of satellite microglia in the somatosensory cortex, striatum, and thalamus in vgat-ires-cre × td tomato × MacGreen transgenic mice. (a–c) Confocal images from the cortex (a), striatum (b), and thalamus (c). Immunolabeling of sections with neuronal marker NeuN (white), Iba-1 antibodies to label the microglia (green), and DAPI (blue) to label nuclei. Transgenic label of vgat td tomato is given in magenta. (a) NeuN labeling is visible in most neuron somata and appears in both the nucleus and cytoplasm, vgat signal (magenta) is confined to a subpopulation of neurons and also labels neurites (arrow). Parenchymal microglia (green), and satellite microglia (arrowheads) attached to NeuN- and vgat-positive neuron. (b) In the striatum, almost all neurons are vgat positive (magenta), arrowhead indicates a microglial cell (green) forming a satellite with a vgat neuron. NeuN is not shown. (c) In the thalamus, vgat transgenic label is visible in neurites (magenta, white arrows) but not found in neuronal somata. Arrowhead indicates a microglial cell (Iba-1, green) forming a satellite (arrowhead) to a NeuN (white)-labeled neuron. Bar 20 μm, valid for a–c. (d–f) One-way ANOVA with Tukey's multiple comparisons test, or two-tailed *t* test applied, as indicated by (f) or *t* values. (d) Quantitative analysis of cell densities (N/mm^3) of microglia, NeuN-positive neurons, and vgat-expressing neurons in the somatosensory cortex (circle), striatum (black diamond), and thalamus (red triangle) by surface rendering with Imaris. Mean ± *SEM* (data from nine to 12 slices and three animals). Microglia density is lower in the thalamus compared to the striatum or to the cortex (**$p = 0.0014$, ***$p = 0.0002$, $F[2, 27] = 12.55$), but not between cortex and striatum ($p = 0.89$). NeuN neuron density is lower in the thalamus compared to the cortex and striatum (****$p < 0.0001$, $F[2, 27] = 20.21$). Vgat neuron density is significantly lower in the cortex compared to the striatum (****$p < 0.0001$; $t[19] = 14.7$); note that in thalamus there are no vgat neuron somata. (e) Percentage (%) of satellite microglia on NeuN neurons (left) and on vgat neurons (right) in the different brain areas; significantly lower % satellite microglia on NeuN neurons in the thalamus versus cortex and striatum (****$p < 0.0001$, $F[2, 27] = 18.3$), no difference between the cortex and striatum ($p = 0.75$); % satellite microglia on vgat neurons is significantly lower in the cortex compared to the striatum ($p < 0.0001$; $t[18] = 12.6$; two-tailed *t* test). (f) Percentage of NeuN neurons (left) and vgat neurons (right) that carry satellite microglia: No significant difference of % NeuN neurons with satellite in the striatum versus cortex ($p = 0.98$), striatum versus thalamus ($p = 0.22$), or cortex versus thalamus ($p = 0.051$, $F[4, 46] = 6.65$); % of vgat neurons with satellites is lower in the striatum compared to those in the cortex (*$p = 0.020$; $t[19] = 2.53$)

Z-dimension was inferred as 50 μm, although the optical thickness could be smaller, due to flattening of the slices. Cell densities were normalized to N/mm^3.

Data describing microglia and neuron densities were obtained from at least three mice and three sections per different brain regions including the somatosensory cortex, striatum, thalamus,

SN, raphe nuclei, and cerebellum. For the comparative analysis in Figure 2, initially four to six rectangular ROIs were analyzed in either region and mean values were calculated for each section, resulting in nine (striatum, thalamus) and 12 data points (cortex). The total number of microglia and specific neurons per brain region was calculated for the imaged volumes and normalized to cells/mm^3. The amount of satellite microglia in a given brain region as based on its contact with a neuron (see above) is presented as percentage of the microglia population. Neurons that are contacted by a microglial cell are also presented as percent neurons with satellite.

2.5 | Distribution analysis of satellite microglia

The distribution of satellite microglia was analyzed in the somatosensory cortex, striatum, and thalamus with the 2D particle distribution plugin of ImageJ (https://imagej.net/plugins/biovoxxel-toolbox; RRID:SCR_015825). Surface-to surface contacts were obtained by Imaris in 3D volumes as described above. Images were captured and binarized, and contacts were considered as individual objects for distribution analysis. According to the ultimate eroded point of the objects and nearest neighbor distances, the macro statistically determines if objects are likely to be randomly distributed, self-avoiding, or build clusters.

2.6 | Statistical analysis

GraphGraphPad prism software (version 7.03) was used for statistical analysis. Data are presented as mean values ± *SEM*, unless otherwise stated. The normal distribution of the data was checked by D'Agostino-Pearson test. Ordinary one-way ANOVA with Tukey's multiple comparisons test was performed to compare the specific cell densities and proportions of satellites in different brain regions. For pairwise comparisons of mean values, we used a two-tailed *t* test. The differences were considered statistically significant at $p < 0.05$ (*), $p < 0.01$ (**), and $p < 0.001$ (***). Pearson correlation coefficient was computed under the assumption of Gaussian distribution with confidence intervals of 95% and choosing a two-tailed *p*-value.

3 | RESULTS

3.1 | Analysis of microglia to neuron contacts using two different approaches

In our study, we analyze the proportion of microglia that form satellites with defined neuronal subtypes in different brain areas and calculate the percentage of a given neuronal subtype being attached to a satellite microglial cell. For that purpose, we obtained confocal *Z*-stacks of fluorescently labeled brain slices from the brain regions of interest. Defined volumes were analyzed by two different bias- and assumption-free approaches, based on Imaris or ImageJ software. They yield absolute cell counts for labeled microglia and neurons per volume and allow to identify the subpopulation of satellite microglia whose cell bodies are in contact with somata of defined neurons. Imaris software was used for analyzing 3D volumes in the cortex, striatum, and thalamus (Figure 1a–d). Surface rendering of neurons and microglia requires a rather homogeneous labeling of the somata. This approach yields information on cell densities in a semi-automated, high-throughput fashion; however, it can only be applied to rectangular volumes (ROIs). For those brain areas, in which the specific neurons are confined to discrete nuclei (raphe nuclei, SN in the basal forebrain) or are arranged in "curved" layers (cerebellar PC layer) (Figure 1e–g), we applied an ImageJ-based approach which allows to analyze irregularly shaped volumes. Transgenic mouse models with genetically labeled glutamatergic, GABAergic, and serotonergic neurons and specific antibodies were used to identify neuronal subtypes. NeuN antibody was used as a pan-neuronal marker and Iba-1 as a microglial cell marker.

The two approaches are illustrated in Figure 1. For analysis with surface rendering, large confocal *Z*-stack scans ranging from the cortex to the striatum were obtained in tile-scan mode (Figure 1a). This covers large areas and allows similar imaging settings for the different brain areas. For subsequent quantitative analysis with Imaris (see Figure 2), four to six rectangular volumes ($320 \times 320 \times 50$ μm^3) that should overlap not more than 30% were randomly selected from the tile scans in the cortex and striatum as illustrated in Figure 1a. A zoomed in confocal image of such a volume analysis is shown in Figure 1b. The microglia are immunolabeled by Iba-1 in green and vgat-tdT-expressing neurons are shown in magenta. A microglial cell body which is in direct contact with a neuronal soma is referred to as satellite microglia, indicated by overlapping fluorescence at the potential contact site. In contrast, microglia whose cell bodies are not attached to a neuronal soma are referred to as parenchymal microglia. For identification and quantification of the percentage of microglia that are satellites to a specific neuron, the Imaris surface-to-surface-contacts tool was used. An example of 3D-rendered microglia and neuron surfaces are shown in Figure 1c, the co-localized cell–cell contact areas on the neuronal surfaces are given in Figure 1d.

As an example for the analysis with ImageJ of an irregular region, we show TH staining of dopaminergic neurons in the SN (Figure 1e). First, irregular shaped areas containing the somata of the neurons of interest were selected with the freehand selection tool and cropped (Figure 1e). The cell counter plugin was applied to manually quantify the neurons and microglia in the cropped *Z*-stacks (Figure 1f). Contacts between microglia closely neighboring a neuron were verified individually in the orthogonal view (Figure 1g).

To test if the Imaris- and ImageJ-based approaches generate comparable cell density data, we cropped irregular areas of the striatum and cortical layers and analyzed the cell densities of microglia and neurons with the ImageJ cell counter plugin in five ROIs. After normalizing the densities to cells/mm^3, we compared those to the values that were generated by the Imaris algorithm for surface

rendering and object identification in the same brain areas. The normalized densities of microglia and of vgat-positive neurons in the striatum, vglut-positive neurons in the layer IV, or NeuN neurons in the layer V of the cortex acquired by both approaches are plotted in Figure 1h. A comparison of the mean values for cell densities obtained by the two quantitative approaches did not yield significant differences (microglia densities in the striatum: 1.256 ± 0.08 vs. 1.062 ± 0.07 × 10^4/mm^3, $p = 0.11$, $t(8) = 1.82$; in layer IV: 1.257 ± 0.12 vs. 1.151 ± 0.05 × 10^4/mm^3, $p = 0.44$, $t(8) = 0.82$; and in layer V: 1.328 ± 0.066 vs. 1.380 ± 0.038 × 10^4/mm^3, $p = 0.51$, $t(8) = 0.68$). Mean values obtained for vgat neuron densities in the striatum did not differ (9.183 ± 0.54 vs. 9.416 ± 0.05 × 10^4/mm^3, $p = 0.76$, $t(8) = 0.32$). Values for vglut neuron densities in layer IV (2.078 ± 0.07 vs. 1.976 ± 0.14 × 10^5/mm^3, $p = 0.53$, $t(8) = 0.65$) and NeuN neuron densities in layer V were comparable (1.232 ± 0.05 vs. 1.150 ± 0.03 × 10^5/mm^3, $p = 0.17$, $t(8) = 1.53$. Also, the amounts of satellite microglia as determined by the two approaches were comparable (% satellite microglia in the striatum: 29.4 ± 3.1 vs. 28.2 ± 1.2%, $p = 0.73$, $t(8) = 0.36$; in layer IV: 53.1 ± 2.9 vs. 56.8 ± 1.5%, $p = 0.29$, $t(8) = 1.13$; and in layer V: 39.9 ± 3.4 vs. 39.4 ± 4.1% $p = 0.92$, $t(8) = 0.11$).

To verify that the two approaches identify similar contacts between microglia and neurons, we performed a side-by-side comparison by Imaris and ImageJ of representative images for a data set from the striatum (Figure S1). We focused on satellite microglia with transgenically labeled vgat neurons. Four randomly cropped volumes were analyzed by IMARIS surface rendering and cell-to-cell contacts were determined. The identical volumes were analyzed in ImageJ by the cell counter plugin and colocalization strategy as described. Results from both approaches match well when comparing them side-by-side. The cell counter strategy detects slightly more contacts which may be explained by the fact that the ImageJ procedure does not set a cutoff value for the area of the contact and may include also contacts that are <50 μm^2. On the other hand, manual counting with ImageJ is prone to human error, especially in the regions of high neuron density. Nevertheless, we feel confident that the data from the two approaches are comparable and can be integrated in one data set.

3.2 | Satellite microglia in the somatosensory cortex, striatum and thalamus of adult mice associate with inhibitory neurons

To study the interaction of inhibitory interneurons with satellite microglia, we used the vgat-ires-cre × td Tomato × MacGreen reporter mice, in which GABAergic interneurons express tdTomato and can thus easily be identified. In this animal model, microglial cells are recognizable by their green GFP fluorescence. Slices were immunolabeled with NeuN as a pan-neuronal marker, with Iba-1 antibody to supplement the intrinsic GFP fluorescence of the microglia and with DAPI to label nuclei.

Quantitative analysis was performed on coronal slices taken between the bregma +1 and 0 which contain the primary somatosensory cortex and striatum (caudate putamen), and on slices between the bregma −1.3 and −1.8 containing the barrel cortex and thalamic areas. Representative examples of confocal images (Figure 2a–c) illustrate that only a subpopulation of all NeuN-positive neurons expresses vgat td Tomato in the somatosensory cortex (both rostral and more caudal areas) (Figure 2a), whereas in the striatum the majority of all NeuN-positive neurons are vgat positive (Figure 2b, NeuN not shown)). In the thalamus, no vgat-positive neuronal somata, but a few vgat-positive projection axons can be observed (Figure 2c). Microglia cells show a homogenous distribution throughout these four analyzed brain areas, and in all regions a subpopulation of microglia can be observed that form satellites with neurons.

The absolute densities of microglia, all neurons (NeuN), and vgat-positive neurons in the 3D volumes were obtained as described, and are given in Figure 2d (and Table 1). To minimize the error due to cell density variability in different cortex layers or due to interspersed white matter tracts in the striatum, four to six rectangular ROIs were analyzed in either region and mean values were calculated for each section, resulting in nine (striatum, thalamus) or 12 (cortex) individual data points (obtained from three mice). Results of statistical analysis and respective tests are given in the legend of Figure 2.

Microglia densities range from 1.27 ± 0.04 × 10^4/mm^3 in the cortex to 1.23 ± 0.08 × 10^4/mm^3 in the striatum to 0.94 ± 0.04 × 10^4/mm^3 in the thalamus. Significant differences were recorded between the cortex and thalamus, and between the striatum and thalamus ($p = 0.0002$ and $p = 0.0014$, respectively, $F[2, 27] = 12.55$, one-way ANOVA). Average neuron density (NeuN) is 1.23 ± 0.037 × 10^5/mm^3 in the somatosensory cortex, 1.32 ± 0.08 × 10^5/mm^3 in the striatum, and significantly lower in the thalamus (0.81 ± 0.05 × 10^5/mm^3) compared to the striatum and cortex (****$p < 0.0001$, $F[2, 27] = 20.21$). The density of vgat-positive neurons is 0.208 ± 0.01 × 10^5/mm^3 in the somatosensory cortex; thus vgat-positive neurons represent a subpopulation of 17% of all NeuN neurons in this area. In the striatum, the density of vgat-positive neurons is 0.92 ± 0.06 × 10^5/mm^3 which is 69% of all neurons (determined by NeuN labeling). The quantification by surface rendering did not reveal vgat-positive cell bodies in the thalamus.

The percentage of microglia that form satellites with NeuN or vgat-positive neurons in the three brain regions is shown in Figure 2e and statistics is summarized in Table 1. In the cortex and striatum, 41.8 ± 1.6% of all microglia form satellites with NeuN-positive cells. In the thalamus, where the absolute density of NeuN-positive neurons is lower, about 24.6 ± 3.3% of all microglia form satellites. Regarding microglia interacting with GABAergic neurons, about 8.2 ± 0.5% of the microglia population in the cortex are satellites to vgat-positive neurons, whereas in the striatum, where the majority of neurons express vgat, about 29.3 ± 1.8% of all microglia form satellites with vgat neurons (Figure 2e). These data suggest that the percentage of satellite microglia correlates with the density of neurons.

The proportion of NeuN-positive neurons that have a satellite microglia is 2.9 ± 0.4% in the thalamus, 4.2 ± 0.3% in the striatum,

TABLE 1 Summary of mean cell densities, normalized to N/mm^3, percentages of satellite microglia and neurons with satellite microglia for the different brain areas, as determined by Imaris surface rendering algorithm or ImageJ cell counter plugin

Brain area	Microglia density	Neuron (soma) density	% satellite microglia	% neuron type with satellite microglia	Approach
Somatosensory cortex (throughout all layers) ($n = 12^*$, $N = 3$)	$1.271 \pm 0.037 \times 10^4$	Vgat: $0.208 \pm 0.010 \times 10^5$	on vgat: $8.2 \pm 0.5\%$	Vgat: $5.8 \pm 0.58\%$	Imaris/Image J
		NeuN: $1.230 \pm 0.051 \times 10^5$	on NeuN: $41.8 \pm 1.6\%$	NeuN: $4.5 \pm 0.22\%$	
(Barrel) Cortex layer IV ($n = 8$; $N = 3$)	$1.344 \pm 0.087 \times 10^4$	Vglut: $2.082 \pm 0.074 \times 10^5$	on vglut: $51.3 \pm 3.1\%$	Vglut: $3.2 \pm 0.13\%$	Imaris
		NeuN: (n.d.)	on NeuN: (n.d.)	NeuN: (n.d.)	
(Barrel) Cortex layer V ($n = 8$; $N = 3$)	$1.459 \pm 0.072 \times 10^4$	Vglut: –	on vglut: –	Vglut: (n.d.)	Imaris/ImageJ
		NeuN: $1.355 \pm 0.087 \times 10^5$	on NeuN: $42.3 \pm 2.4\%$	NeuN: $4.4 \pm 0.27\%$	
Striatum ($n = 9^*$; $N = 3$)	$1.237 \pm 0.075 \times 10^4$	Vgat: $0.924 \pm 0.055 \times 10^5$	on vgat: $29.3 \pm 1.7\%$	Vgat: $3.9 \pm 0.29\%$	Imaris/ImageJ
		NeuN: $1.323 \pm 0.080 \times 10^5$	on NeuN: $44.3 \pm 2.5\%$	NeuN: $4.2 \pm 0.34\%$	
Thalamus ($n = 9^*$; $N = 3$)	$0.940 \pm 0.036 \times 10^4$	Vgat: 0.0	–	Vgat: –	Imaris
		NeuN: $0.814 \pm 0.037 \times 10^5$	on NeuN: $24.6 \pm 3.3\%$	NeuN: $2.9 \pm 0.43\%$	
Raphe nucleus ($n = 8$; $N = 5$)	$0.64 \pm 0.07 \times 10^4$	Serotonerg: $0.14 \pm 0.03 \times 10^5$	on serot.: $2.4 \pm 1.0\%$	Serotonerg.: 1.2%	ImageJ
Substantia Nigra (SNC) ($n = 9$; $N = 3$) (SNR)	$0.89 \pm 0.08 \times 10^4$	Dopaminerg: $0.31 \pm 0.02 \times 10^5$	on dopam.: $8.96 \pm 2\%$	Dopaminerg: 2.3%	Image J
	$1.95 \pm 0.18 \times 10^4$	–			
Cerebellum (all layers) Purkinje cell layer ($n = 15$; $N = 3$)	$0.432 \pm 0.054 \times 10^4$	–	–	–	ImageJ
	–	Purkinje cells: $0.99 \pm 0.06 \times 10^5$	on PC: $39.5 \pm 8.5\%$	Purkinje: 3.3%	

Note: All values represent mean values of cell density ± *SEM*, normalized to N/mm^3, * data points generated by averaging values obtained from two to four ROIs/slice. *n*, number of data points (analyzed slices); *N*, number of animals.

and 4.5 ± 0.2% in the cortex. In the cortex, 5.8 ± 0.6% vgat-positive neurons have a satellite microglia, while in the striatum, 3.9 ± 0.3% of vgat neurons have a satellite, and the difference is significant (*$p = 0.02$; $t[19] = 2.53$; two-tailed t test).

To test whether the distribution of satellite microglia follows certain patterns or is rather homogeneous, we used surface rendering data from the cortex, striatum, and thalamus and the resulting cell-to-cell contacts as indicator for satellite microglia. The 3D images of contacts obtained by IMARIS for nine randomly selected volumes ($340 \times 340 \times 50$ μm^3) in each area were captured and analyzed by the ImageJ "particle distribution plugin (2D)". The tool statistically determines if these objects (according to their ultimate eroded point) in a 2D image are likely to be randomly distributed, self-avoiding, or build clusters. Based on the median nearest neighbor distance (NND) with a confidence interval of 95%, this analysis indicated a "random particle distribution" in almost all analyzed areas in the cortex and striatum. The average theoretical random NND values determined for the cortex and striatum were 78.5 ± 13.5 μm (± *SD*) and 77.3 ± 12.0 μm (± *SD*), respectively. The analysis in the thalamic areas with lower object densities and an average NND value of 157.3 ± 34.9 μm (± *SD*) revealed "self-avoiding particles" in the majority of cases. This analysis indicates that the distribution of satellite microglia in the tissue is rather homogeneous, and does not follow tissue architectural cues. However, in areas with no neuron somata, such as white matter regions one would hardly detect any satellite microglia.

In conclusion, in the three brain areas, satellite microglia associate both with GABAergic and non-GABAergic neurons in a density-dependent fashion, with their number lower in the thalamus, a region with lower neuron density.

3.3 | Layer-specific analysis of satellite microglia in the somatosensory cortex of vglut-ires-cre × tdT mice

To analyze the interaction of satellite microglia with glutamatergic neurons, we employed a transgenic mouse strain that shows the expression of tdTomato in vglut-2 neurons and GFP label in microglia. In these animals, a subpopulation of neuronal cell bodies in layers II–IV of the somatosensory cortex and in the hippocampal dentate gyrus and CA1-3 area show vglut tdTomato signal (Figure 3a). We compared satellite microglia density in layers IV and V of the cortex as models for glutamatergic and non-glutamatergic neurons, respectively. The pyramidal neurons in layer V can be labeled by NeuN but are negative for vglut tdTomato. While microglia appear homogeneously distributed throughout the layers of the cortex, there is a variation regarding neuronal soma size and density throughout the layers (Figure 3b–d). The soma identification of vglut-positive neurons through 3D rendering by Imaris is hampered in layer IV, since in this layer the vglut-transgenic signal is not only confined to the neuronal somata but is also expressed by dendrites. Therefore, we used the colocalization tool to overlay vglut tdTomato signal with NeuN fluorescence and subsequently created neuron surfaces from the colocalization channel. Figure 3e,f show examples for 3D surface rendered vglut-positive neurons in layer IV and NeuN-positive neurons and microglia in layer V. Absolute cell densities [after normalization to cells/mm^3] as obtained by Imaris surface rendering analysis are given for microglia in Figure 3g. Average microglia densities are $1.34 \pm 0.09 \times 10^4$/mm^3 in layer IV and $1.46 \pm 0.07 \times 10^4$/mm^3 in layer V, and not significantly different (n = 8 (N = 3), $p = 0.32$, $t(14) = 1.02$; unpaired t test). These values correspond to the density that was obtained for the entire somatosensory cortex in the vgat mouse model (Figure 3g, all layers). The absolute cell density of vglut-positive neurons in layer IV was $2.08 \pm 0.074 \times 10^5$/mm^3 and hence almost twice as high as the cell density of (NeuN-positive) somata in layer V ($1.35 \pm 0.087 \times 10^5$/mm^3). For a comparison, Figure 3 H also shows the overall density of vgat- and NeuN-positive neurons in the somatosensory cortex (as shown in Figure 2). The percentage of microglia that form satellites with vglut-positive neurons in layer IV, and with NeuN neurons in layer V was assessed as described above and is shown in Figure 3 I. In layer IV, 51.3 ± 3.1% of all microglia are satellites to vglut neurons, whereas in layer V, on average, 42.3 ± 2.4% of all microglia form satellites to NeuN neurons. This corresponds to the proportion of satellite microglia determined across all cortical layers (data for Figure 2), and is shown as separate column in Figure 3i. Comparing the mean values of absolute neuron densities and percent satellite microglia (Figure 2h,i) is suggestive of a correlation between neuronal density and the fraction of satellite-forming microglia. 4.4 ± 0.27% of the NeuN-labeled neurons in layer V have satellite microglia, whereas the percentage of satellites on vglut neurons in layer IV is slightly lower (3.2 ± 0.13%) and significantly different ($p = 0.0015$, $t(14) = 3.92$, unpaired t test) (Figure 3j).

3.4 | Microglia can form satellites to serotonergic neurons in the raphe nuclei of the brain stem as a rare event

A transgenic mouse model expressing eYFP under the control of the Tph2 (tryptophan hydroxylase 2) promoter (Zhao et al., 2011) was used to investigate the satellite microglia associated with serotonergic neurons. Serotonergic neuron cell bodies are located in the raphe nucleus of the brain stem from where they project axons to different brain areas. Both somata and axon projections can be identified due to their green fluorescence (Figure 4). Microglia were labeled with Iba-1 and visualized by a red fluorescent secondary antibody. NeuN was used as a pan-neuronal marker. Due to the small size and irregular shape of the brain nucleus, and due to the strong labeling of the serotonergic projections that originate from the raphe nucleus (Figure 4a), quantification by the Imaris algorithm was not applicable and the ImageJ-based approach was applied. In total, nine cropped *Z*-stacks containing the raphe nuclei (from five animals) were analyzed, which corresponded to a total analyzed volume of 0.034 mm^3. As can be appreciated from Figure 4a, NeuN-positive neurons outnumber the Tph2-EYFP-positive neurons in the raphe nucleus. We

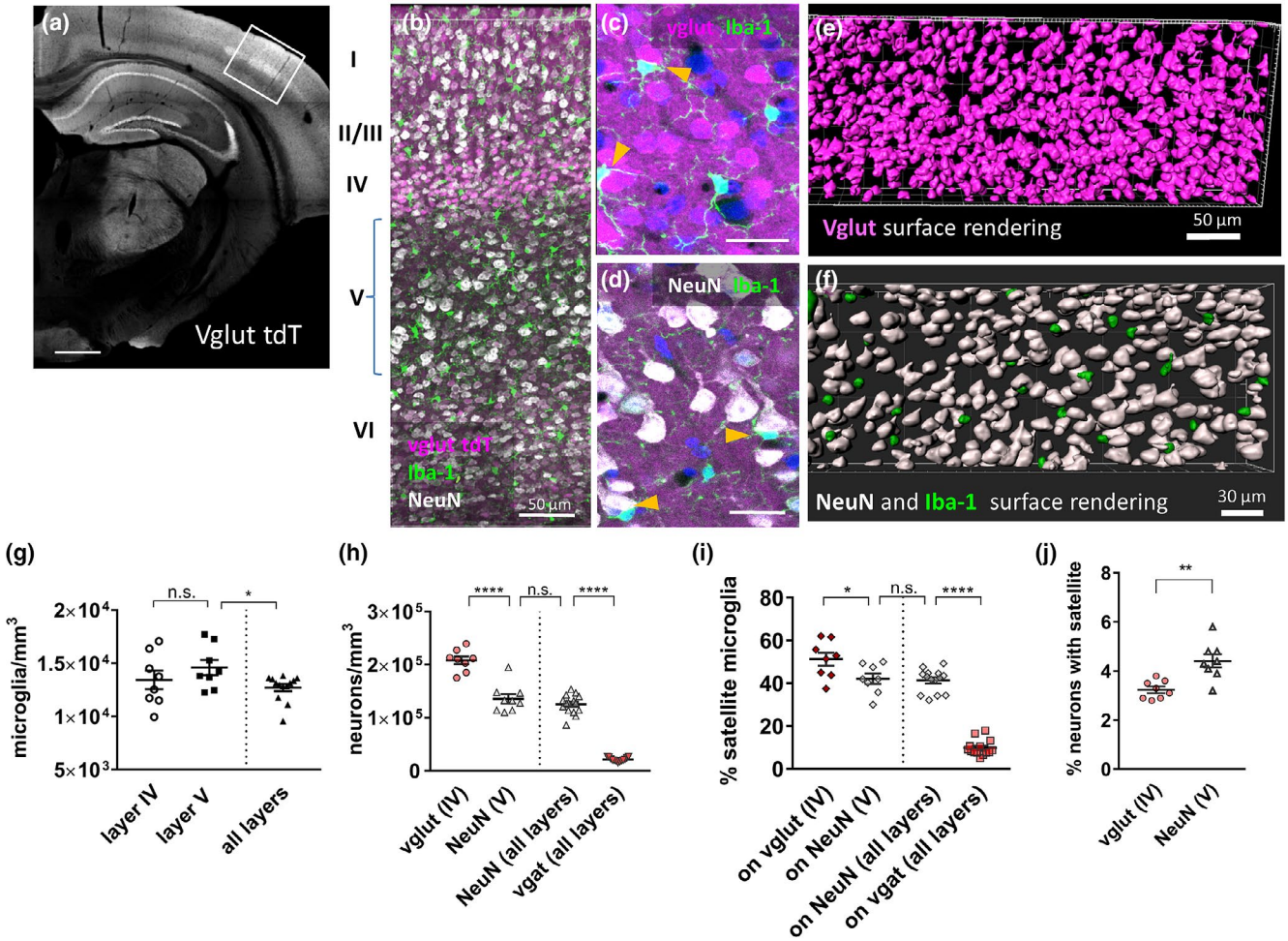

FIGURE 3 The analysis of satellite microglia with glutamatergic neurons in specific layers of the somatosensory cortex of vglut-ires-cre × tdT mice. (a). Overview scan of a cortical hemisphere of a coronal section of a vglut-ires-cre × tdTomato × Macgreen eGFP mouse (vglu tdT) illustrates vglut-expressing neuronal cell bodies mainly in layer IV of the somatosensory cortex, and in the hippocampal pyramidal cell layers and dentate gyrus. (b). Imaris 3D views of a scanned *z*-stack through somatosensory cortex showing overlay of vglut-tdT signal (magenta), Iba-1/Macgreen eGFP (green), and NeuN staining (white) of all neurons; the numbers on the left indicate cortical layers. (c). Confocal image showing vglut neurons (magenta) in layer IV. Microglia (green) indicated by arrowheads form satellites to vglut neurons. (d). Confocal image showing pyramidal neurons in layer V, labeled with NeuN (white). Some microglia (green) form satellites with pyramidal neurons (arrowheads). Magnification bars: 500 µm in a; 50 µm in b and e; 20 µm in c and d; and 30 µm in f. (e). 3D images of rendered vglut neuron surfaces in layer IV. (f). 3D image of layer V after surface rendering of NeuN-labeled neurons and Iba-1/Macgreen-labeled microglial cell bodies (green). (g–j) Scatterplots show quantitative data obtained by Imaris analysis (mean ± *SEM*). (g) Microglia density in layer IV, layer V, and averaged over all cortical layers (as given in Figure 2); density in layer IV versus layer V ($p = 0.44$), layer IV versus all layers ($p = 0.67$), and layer V versus all layers ($^*p = 0.08$; $F[2, 26] = 2.52$; one-way ANOVA with Tukey's multiple comparisons). (h) The densities of vglut neurons in layer IV, NeuN cell density in layer V. For a comparison, the density of vgat and NeuN neurons in the somatosensory cortex averaged over all layers (as given in Figure 2) is shown. Average values for NeuN density in layer V versus all layers do not differ ($p = 0.27$, $t(22) = 1.13$; two-tailed *t* test). (i) Percent satellite microglia with vglut neurons (in layer IV) and with NeuN neurons (in layer V) ($^*p = 0.36$, $t(14) = 2.3$, two-tailed *t* test); for a comparison, the percentage of satellite microglia with vgat neurons (red squares) is smaller than with NeuN neurons (gray diamonds) averaged over all cortical layers ($^{****}p < 0.0001$, $t[26] = 18.0$). (j) Percent neurons that carry a satellite microglia ($^{**}p = 0.006$, $t[29] = 2.97$, two-tailed *t* test)

counted a total of 421 Tph2 neurons corresponding to a mean neuronal density of $1.4 \pm 0.3 \times 10^4/\text{mm}^3$, and 201 microglia, which corresponds to a mean microglial density of $0.64 \pm 0.07 \times 10^4/\text{mm}^3$. Only five microglial cells were found in close apposition to a soma of a serotonergic neuron resulting in a percentage of 1.2% of all serotonergic neurons that have a satellite. Among the entire microglia population, a proportion of 2.4% of all microglia are satellite microglia to a serotonergic neuron in this brain area (Table 1).

3.5 | Dopaminergic neurons in the substantia nigra can associate with satellite microglia

Next we assessed whether and to what extent microglia establish satellites with dopaminergic neurons. Coronal sections containing the SN and ventral tegmental area were immunostained with antibodies to tyrosine hydroxylase (TH). TH-positive dopaminergic neurons were located in the SN pars compacta (SNC), whereas in

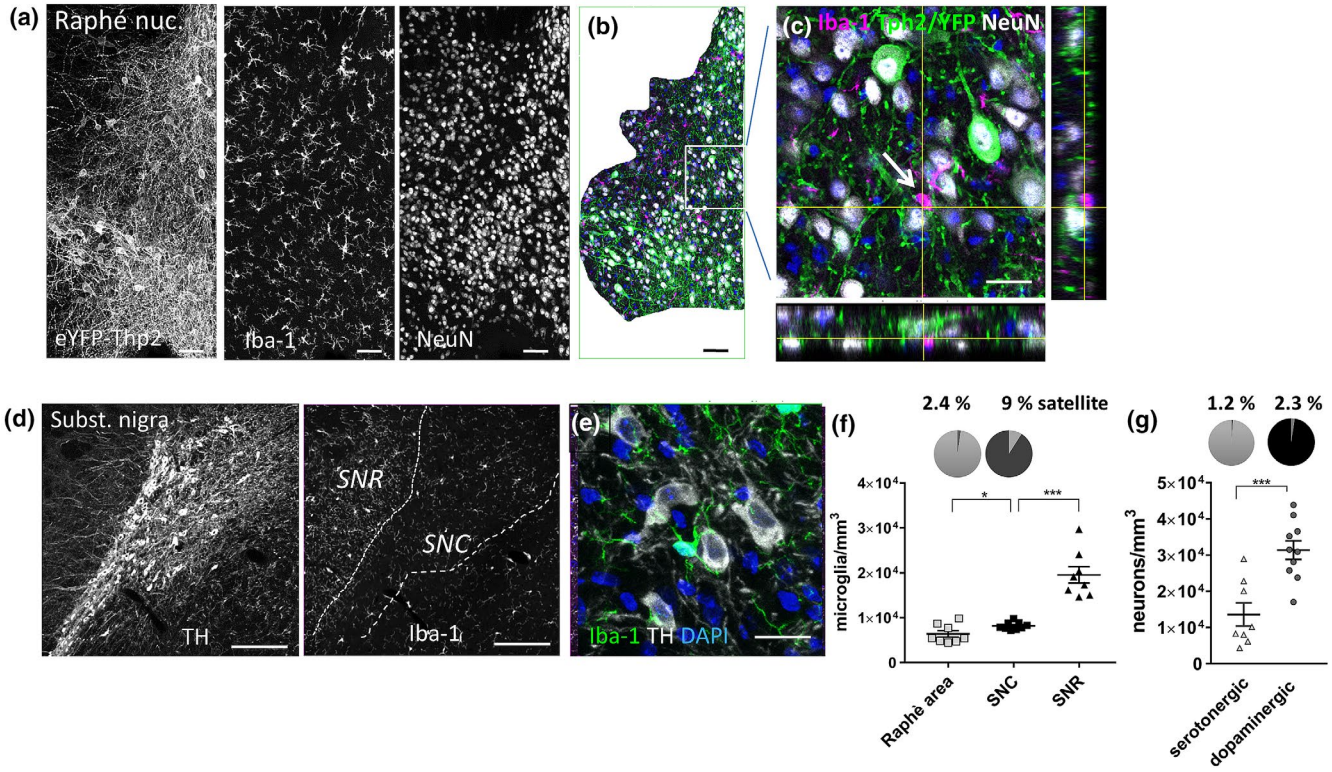

FIGURE 4 Microglia form satellites on serotonergic neurons in the raphe nucleus and on dopaminergic neurons in the substantia nigra. (a). Coronal section with the raphe nucleus from an eYFP-Tph2 transgenic mouse. Serotonergic neurons and their dense network of projections are visible due to their intrinsic fluorescence (left). Microglia are labeled by Iba-1 (middle), NeuN is used as a pan-neuronal marker (right). (b). Cropped area containing Thp2 neuron somata for cell counter analysis; overlay image of all markers (note: microglia are shown in magenta, Thp2 neurons in green, and NeuN in white). (c). Blow-up of framed area in b, and orthogonal view to identify an Iba-1-stained microglia (magenta) (arrow) as a satellite of a serotonergic neuron (green and white). Magnification bars: 50 μm in a, b; 20 μm in c. (d). Coronal brain sections with the substantia nigra from C57Bl/6 mouse immunostained for tyrosine hydroxylase (TH), which labels dopaminergic neurons and projections. TH-positive somata were located mainly in the substantia nigra pars compacta (SNC), whereas in the major output nucleus substantia nigra pars reticulata (SNR) contains mainly dopaminergic striatal projections (left panel). Iba-1 labeling shows that microglia density is reduced in SNC compared to SNR (right panel). (e). Higher magnification to show an example of an Iba-1-positive microglia (green) contacting a TH-positive neuron (white). Magnification bar: (d) 100 μm, (e) 20 μm. (f) Scatterplot of microglia cell density in the substantia nigra pars compacta (SNC) and pars reticulata (SNR) ($n = 9$ ROIs, $N = 3$) and raphe nuclei ($n = 8$ ROIs, $N = 5$); line indicates mean ± *SEM* (*$p = 0.03$, $t(15) = 2.40$; ***$p < 0.0001$, $t(14) = 6.55$, two-tailed *t* test). Pie charts above indicate percentage of satellite microglia on serotonergic (gray) and dopaminergic neurons (black). (g). Scatterplot of neuron density in the raphe nuclei (serotonergic) and substantia nigra (dopaminergic), determined by cell counter plugin (mean ± *SEM*, ***$p = 0.0005$, $t[16] = 4.38$, two-tailed *t* test). Pie charts on top illustrate the percentage of serotonergic (gray) and dopaminergic neurons (black) that have a satellite microglia

the SN reticulata (SNR) only weakly labeled projections were visible (Figure 4d). The TH-labeled dopaminergic neurons show a donut-like appearance since the antibody labels mainly the cytoplasm and spares the nuclear region (Figure 4e). For the reasons mentioned above, the densities of dopaminergic neurons and microglia were analyzed in selected areas by the ImageJ cell counter plugin; satellite microglia were tracked manually in orthogonal views. Ten brain sections from three animals were analyzed in a total volume of 0.07 mm^3. The mean density of TH-positive neurons in SNC was determined as $3.1 \pm 0.2 \times 10^4/mm^3$ and the microglia density was $0.89 \pm 0.08 \times 10^4/mm^3$ in the same area. Among a total of 2212 TH-positive neurons, 52 were associated with a satellite microglia, corresponding to 2.3%. In the same volume we counted 628 microglia, 52 of those were satellites to a dopaminergic neuron, corresponding to 9% of the total microglia population. The absolute densities of microglia in the raphe nuclei and in the SN and the densities of neurons are summarized in Figure 4f,g and Table 1. The percentages of satellite microglia and neurons with satellite microglia, respectively, are indicated.

3.6 | Large cerebellar Purkinje neurons can be accompanied by satellite microglia

Next we analyzed the spatial relationship of microglia with Purkinje cells in the cerebellum. Purkinje cells are GABAergic neurons and are among the largest neurons in the CNS. Their somata are confined to a single layer and they extend their elaborate dendritic tree into the

molecular layer. We used 50 μm thick sagittal cerebellar sections of vgat-ires-cre tdTomato × MacGreen mice that had been labeled with Iba-1. Purkinje neurons and numerous small inhibitory interneurons of the molecular layer display a strong transgenic vgat signal (Figure 5a,b). For a comparison, the labeling pattern of glutamatergic neurons in the cerebellum of the vglut-transgenic animals was complementary, with vglut being expressed by all granule cells and a few neurons in the molecular layer (Figure 5a, right panel). The average density of microglia was determined in confocal *Z*-stack images (15 slices from three animals) throughout the granule, Purkinje cell, and molecular layer by ImageJ cell counter plugin. Microglial density was on average $0.43 \pm 0.05 \times 10^4/mm^3$. Microglia are less densely

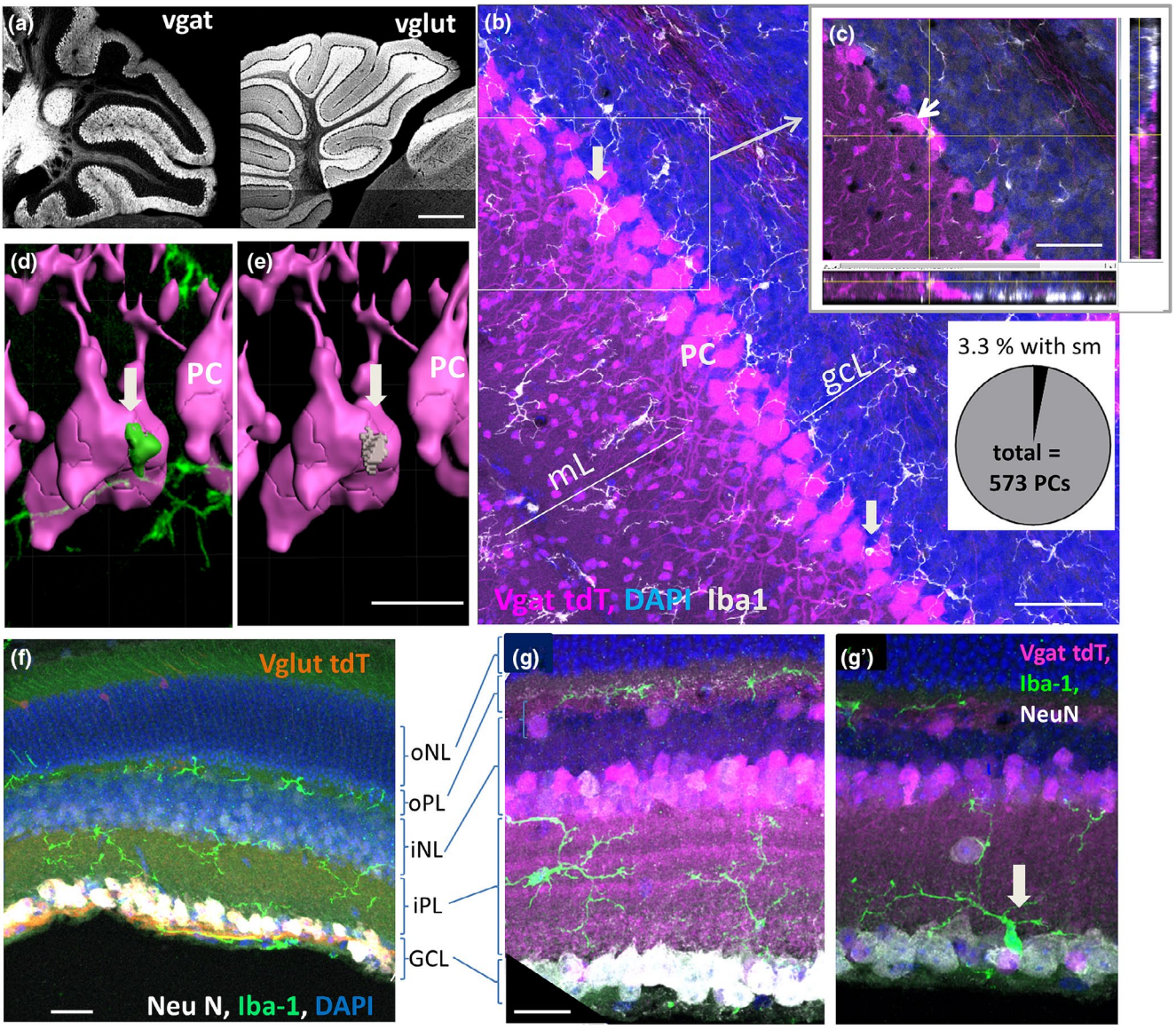

FIGURE 5 Satellite microglia in the cerebellar cortex and in the retina. (a) Overview of vgat and vglut expression, markers show inverse distribution in the cerebellar cortex; (b) Projection image of a 30 μm confocal *z*-stack of a section of vgat-ires-cre × tdTomato × Macgreen transgenic mouse; Purkinje cells (PC), stellate and basket cells in molecular layer (ml) express vgat (magenta); granule cell layer (gcL) is devoid of vgat signal. Microglia are displayed in white; DAPI (blue); fat arrows mark two satellite microglia on PCs; (c) Confocal section as outlined in b of the same stack and orthogonal views indicate that the microglia is in direct contact with the PC soma. (d,e) Identical 3D views of Imaris surface rendering of vgat × tdTomato-positive PC neurons and Iba-1-positive microglia (green). In e, microglia are masked, instead the cell–cell contact area is given in gray (arrow). Magnification bars: 500 μm in a; 50 μm in b and c; and 20 μm in d and e. (f) Transverse sections through the retina of vglut-ires-cre × tdTomato transgenic mouse. Microglia (green) reside within the plexiform layers, and rarely in the ganglion cell layer (GCL); GC neurons express vglut transgene (red) and are NeuN positive. Bipolar neurons in the inner nuclear layer (iNL) and photoreceptor cells in the outer NL show weak or no NeuN expression. (g) Max. projection image of transverse section of a vgat-ires-cre × tdTomato transgenic mouse; microglia (green) reside in plexiform layers (iPL, oPL). (g') Confocal image showing a rare example for a microglial cell in direct contact with a ganglion cell soma (arrow). Magnification bars: 20 μm in f–g'

distributed as compared to other brain areas, thereby confirming the findings of Lawson et al. (1990) who described that microglia in the cerebellum are by a factor 3–4 less densely packed than in some mesencephalic or cortical areas. The formation of satellite microglia with vgat-positive Purkinje neurons can be shown by the Imaris 3D surface rendering (Figure 5d,e). To assess satellite microglia formation, we restricted the quantitative analysis to the Purkinje cell layer by manually cropping and counting microglia and Purkinje neurons in the cropped *Z*-stacks by ImageJ as described. In the analyzed volumes, we counted 573 Purkinje cell neurons of which 19 were associated with a satellite microglia, corresponding to 3.3% of all Purkinje neurons. In the same volume, we counted 45 microglia somata, of which 18 were in direct contact to a Purkinje cell neuron, which corresponds to a proportion of 40% satellite microglia.

3.7 | Retinal microglia can form satellites with neurons of the ganglion cell layer

Like in other regions of the CNS, microglia in the retina constitute a prominent part of the resident glial population and display a ramified morphology (Lee et al., 2008). One distinguishing feature, however, is their stratified distribution in the inner and outer plexiform layers where neuronal synapses are formed and their absence from the nuclear layers with neuronal cell bodies in the normal mouse retina (Hume et al., 1983; Karlstetter et al., 2010) which would imply that soma–soma interaction and formation of satellite microglia does not occur in the normal retina. Transverse cryosections or whole mounts of the retinae from vgat- and vglut-transgenic mice were immunostained with Iba-1 and with NeuN antibodies to identify satellite microglia. As illustrated in transverse sections, the vglut signal is confined to the ganglion cells (Figure 5f), whereas vgat-positive neurons, probably inhibitory interneurons, are found in the inner nuclear layer and rarely in the outer nuclear and ganglion cell layers (Figure 5g,g'). NeuN antibody labels retinal ganglion cells but does not label the neurons of the other layers which has been described before (Gusel'nikova & Korzhevskiy, 2015). Iba-1-positive microglia reside within the plexiform layer, their processes interact with synapses, and can stretch out into the nuclear layers. When a microglial cell body is located close to the border of plexiform layer, it can attach to a neuronal soma and form a satellite (Figure 5g'). We observed satellite microglia both with ganglion cells and with neurons of the inner nuclear layer, and they associate both with vgat- or vglut-positive neurons.

3.8 | Synopsis of all quantitative data suggests a correlation between satellite formation and neuron soma density

The results so far did not indicate a preference of satellite microglia for a specific neuronal subtype but rather suggest that steric factors and histo-architecture determine the amount of satellite microglia present in a given area. Since we proved that the disparate image analysis approaches yield comparable numerical data, we feel confident to combine all data and test if there is a correlation between numerical density of neurons and the amount of satellite microglia formed. Microglia and neuron numerical densities are summarized in Figure 6a and Table 1. Microglia densities show little variation across the different areas and their absolute values correspond well to values determined before (Keller et al., 2018), with the exception of the cerebellum, where their density is by a factor 3–4 lower, and the SNR, where microglia density clearly exceeds that of the neighboring SNC. Region-specific variations across basal ganglia have also been reported in a previous study by De Biase et al. (2017).

Absolute neuron densities are summarized in Figure 6b and vary considerably depending on their functional category (inhibitory or excitatory neurotransmitters) and according to brain region and histo-architectural organization. The neuron/microglia ratios (Figure 6c) show by what factor the neurons outnumber the amount of microglia in the analyzed areas; for instance, in layer IV of the somatosensory cortex, the absolute number of vglut neurons is about 15 times higher than the number of microglia (Figure 6c). Figure 6d summarizes the percentages of satellite microglia on specific neurons in all areas. The scatterplot in Figure 6e shows all data for percent satellite microglia to certain neuronal subtypes in a given brain region as a function of the absolute neuron density in that brain area. Modeling the causal relationship of the nine pairs of values by a linear regression model suggests an almost linear correlation of these two parameters with Pearson correlation coefficient of $r = 0.944$ (95% CI = 0.751 to 0.99, $p = 0.0001$). In conclusion, the amount of satellite microglia in a given brain region is rather determined by steric factors, namely the absolute density of neurons in that area, and there is apparently no preference to form satellites to neuronal subtypes. The higher the abundance of a given neuronal subtype, the higher the probability of a microglial cell body being located in the close vicinity of a neuron soma.

4 | DISCUSSION

In his landmark series of papers, Hortega described and defined microglia and also inferred the term "satellite microglia" for microglial cells which have a close soma-to-soma relationship with neurons. He found these cells in the cortex, cerebellum, and in the medulla oblongata. He reported that when these cells are located at the base of the neuron, their appendages are directed upward and are attached to the neuronal soma by wrapping it like a basket. When they are positioned at the edges of the pyramidal cell body or near its main process, they stretch in the same direction and accompany it for quite some distance (Del Rio Hortega, 1919; Sierra et al., 2016, 2019). Besides microglia associated with neurons, he also described the associations of microglia with vascular structures and with astrocytes (Del Rio Hortega, 1919; Sierra et al., 2016). In case of "vascular satellites," he probably referred to parenchymal microglia or to pericytes located in the perivascular space. To our knowledge, there is no

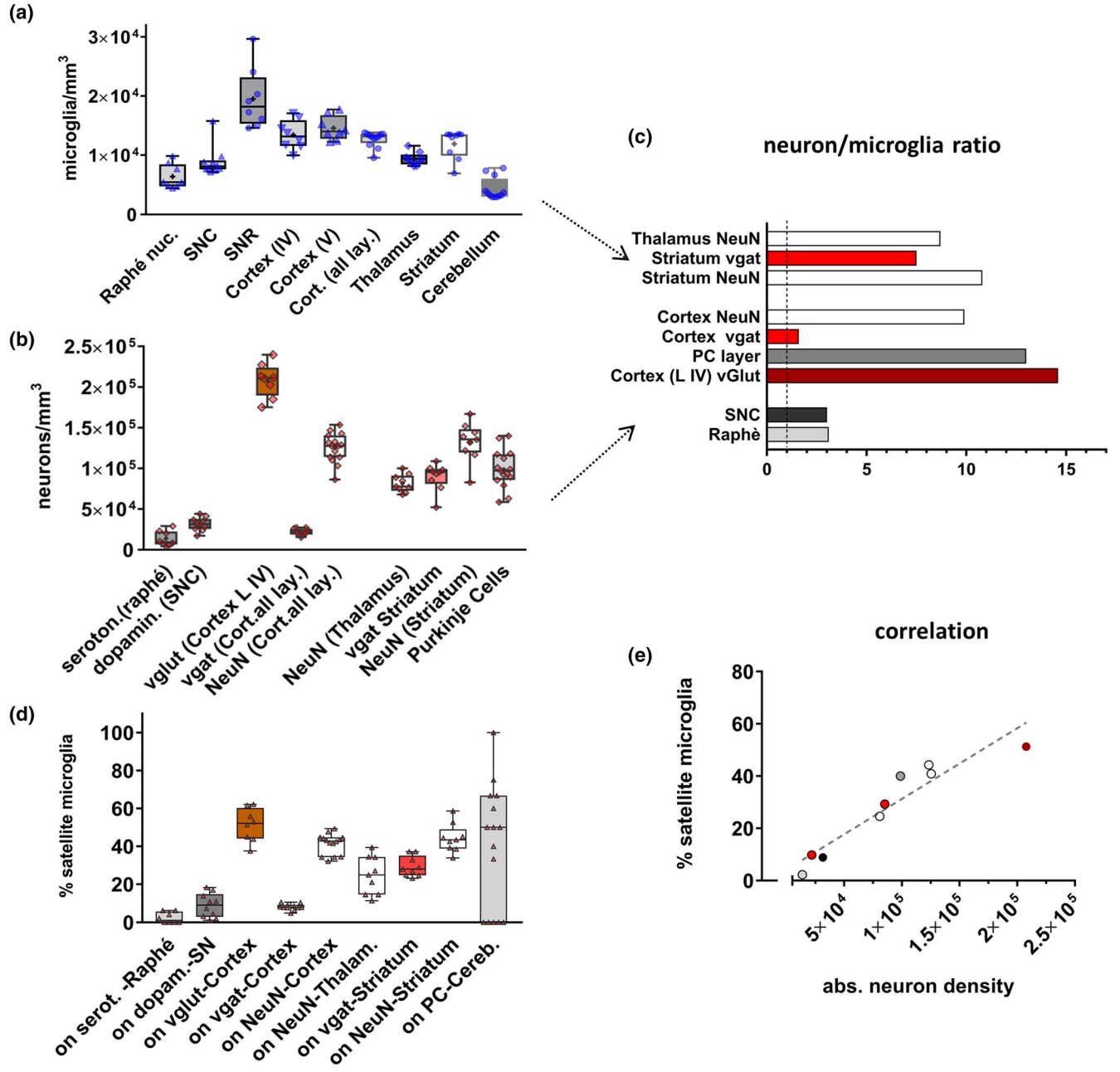

FIGURE 6 Synopsis of quantitative data suggests a correlation between neuronal density and percentage of satellite microglia. Box plot overlays (a,b,d) summarizing numerical densities of microglia (a) neuron types (b), and % satellite microglia (d) as obtained for Figures 2–5 across the different brain areas (as indicated). Data are presented as boxes showing median (line), mean (+), and quartiles (25% and 75%, box). The whiskers extend to the highest and lowest values. (c) Bar graph illustrates neuron/microglia ratios for the same areas as given in a and b. (e) Scatterplot showing the correlation between the density of neurons in a given brain area and the percentage of satellite microglia. Colors of data points correspond to colors of columns in b and d. Pearson correlation coefficient $r = 0.944$ (95% CI = 0.75 to 0.99, $p = 0.0001$)

evidence that a subpopulation of microglia is associated with astrocytes. However, an association of microglia with adult neuronal stem cells has been reported (Su et al., 2014). During development, direct interaction can be indicative for phagocytosis, and indeed microglia can engulf neuron precursors during neurogenesis (Kaur et al., 2007).

After Hortega's initial observation, this neuron microglia association has only recently been further investigated. A special type of microglia with a close association with the axon initial segment has been described in the cortex which can be viewed as a subpopulation of the satellite microglia named AXIS microglia (Baalman et al., 2015). Using a transgenic reporter mouse that expressed tdTomato in GABAergic neurons, they found that 1% of GABAergic neurons (which make up 15% of neurons in adult M1 cortex) had AXIS microglia attached to them, whereas 2% of non-GABAergic neurons had AXIS microglia. They concluded this particular type of satellite microglia preferentially interacts with non-GABAergic neurons.

In previous studies, our group has explored whether the satellite microglia sense the neuronal activity of its partner neuron by dual patch clamp experiments of associated cell pairs in the cortex and hippocampus, but failed to record such interactive activity (Wogram et al., 2016). Evoked local field potentials or action potentials and postsynaptic potentials of the associated neuron did not lead to any transmembrane currents or non-capacitive changes in the membrane potential of the satellite microglia.

Here, we addressed the question whether satellites are formed between microglia and defined neuronal subtypes. We therefore analyzed the potential interaction of GABAergic, glutamatergic, serotonergic, and dopaminergic neurons in different brain regions with satellite microglia. By combined transgenic- and immunolabeling of neurons and microglia in the normal adult murine brain tissue and three-dimensional imaging and analysis approaches, we quantified satellite microglia with GABAergic and glutamatergic neurons in the somatosensory cortex, striatum, and thalamus; with dopaminergic and serotonergic neurons in the basal forebrain and raphe nucleus, respectively; and with the cerebellar Purkinje cell neurons. Satellite microglia in the retina were also assessed, however only in a qualitative manner. They were observed in all analyzed areas. A preference for a specific neuron subtype was not found. The occurrence and frequency of satellite microglia is rather determined by the histoarchitectural organization of the brain area and the densities of neuronal somata therein. Our results indicate that satellite microglia have the potential to interact with all these subtypes of neurons.

The quantitative approaches employed in our study rely on fluorescence detection by cell-specific immunolabeling and transgenic markers to define cell densities and surface–surface contacts in 3D volumes. Transgenic signals of vglut and vgat tdTomato provide a strong labeling of the neuron cytoplasm which allowed rendering of the somata. NeuN also provided a useful label since it is localized in nuclei and perinuclear cytoplasm (Gusel'nikova & Korzhevskiy, 2015). However, notable exceptions have been reported, including Purkinje cells in the cerebellum, and many neurons in the retina that do not express the protein. NeuN is also not a reliable marker for dopaminergic neurons in SN (Cannon & Greenamyre, 2009). Further, impaired penetration of NeuN antibodies into the deeper layers of the tissue sections, in particular in brain regions of high soma density, hampered uniform surface rendering throughout the 3D stacks and may have led to the underestimation of NeuN cell density and, consequently, of the number of contacts between NeuN-positive neurons and microglia. This potential imprecision in the surface rendering approach could be partly compensated for in the section-wise manual counting approach in ImageJ, by adjusting brightness in deeper section layers. Another cause of concern arises from the measurements of section thickness and the vertical shrinkage of the mounted sections. This phenomena and different sources for variations have been extensively discussed by Dorph-Petersen et al. (2001) who note that differential tissue shrinkage and compression in the z-axis occur in frozen-cut sections. In our study, we observed an amount of shrinkage in vertical direction that corresponded well to the value reported by Bermejo et al.(2003). Thus, we were confident to infer a thickness in Z-direction of 50 μm to calculate the volumes. Another source of impreciseness may originate from manual delineation of the counting units in the raphe, SNR nuclei, and cerebellar Purkinje cell layer. By our approach, we do not claim to provide exact stereological data for cellular densities. Nevertheless, the obtained data match amazingly well with anatomical data from other studies for densities of neuron subtypes and microglia as summarized by Keller et al. (2018).

As already noted by Hortega, microglia are ubiquitously distributed throughout the adult CNS, with [minor] regional density variations (Del Rio Hortega, 1919; Keller et al., 2018; Lawson et al., 1990). They are intercalated in neuropil, myelinated tracts as well as neuronal layers and their morphological and functional diversity is determined by local cues (De Biase et al., 2017; Kapoor et al., 2016; Zheng et al., 2021). In contrast, the density of neurons across brain regions can considerably differ (Keller et al., 2018), depending on the neuron size and spatial organization. Our study revealed a positive correlation between the density of certain neuron somata in a given area and the percentage of satellite microglia. Microglia residing in neuropil layers, such as in the plexiform layers of the retina, can form satellites only in cases where their cell bodies reside in the periphery of that layer and sterically close to the somata of neighboring neuron layers. Consequently, microglia in white matter tracts are by definition parenchymal microglia.

Sex differences occur throughout the entire brain (McEwen & Milner, 2017); recent research has shown a sexual dimorphism in microglia isolated from male and female brains in transcriptomic and proteomic profiles, in their signaling and neuro immune function (Guneykaya et al., 2018). Across development, microglia density and morphology can vary between the sexes and these differences in microglia density can persist in the adult stage (Nelson et al., 2019). While the present study analyzed satellite microglia only in male animals, future studies need to prove whether also satellite microglia formation is under the influence of sex hormones.

A direct soma–soma interaction with neurons has also been described for macroglia. In gray matter areas like the cortex, myelinating satellite oligodendrocytes can be observed in close apposition to the soma of neurons in the cortex and they preferentially associate with glutamatergic neurons (Battefeld et al., 2016; Takasaki et al., 2010). Satellite oligodendrocytes with layer V pyramidal neurons locally shape the intrinsic excitability and rhythm in neuronal circuits through regulating extracellular K^+ and Ca^{2+} concentrations (Battefeld et al., 2016). Ion buffering in the perisomatic domain is possible because oligodendrocytes are integral component of an electrically coupled glial syncytium. Satellite microglia, in contrast, are not part of the glia syncytium (Richter et al., 2014) and are also not dye-coupled to the associated neuron (Wogram et al., 2016).

The present morphological survey comprises a snapshot in time of this specific neuron–microglia interaction and therefore does not provide insights into the dynamics of the contact. Previous two-photon imaging studies show that microglia in intact brains in vivo are highly dynamic (Davalos et al., 2005; Dibaj et al. 2010; Nimmerjahn et al., 2005). However, the microglial

processes are in continuous motion whereas cell bodies remain morphologically stationary over hours. Also neuronal somata do not show any translocation over hours. These observations suggest that soma–soma interactions between microglia and neurons are rather stable in intact tissue. Further noninvasive studies involving models with fluorescently labeled cytoplasmic membranes and high-resolution in vivo imaging are required to corroborate this assumption and to rule out small movements of the microglia soma that could easily terminate close cell–cell contacts. Since the microglia–neuron contact can be lost after activation due to brain injury, as show for axon initial segment microglia, such specific interaction is probably part of normal, non-pathologic brain function (Baalman et al., 2015).

A study on the formation of satellite microglia during development may provide further insights into the dynamics of microglia–neuron interactions. Baalman et al. (2015) investigated this developmental aspect for AXIS microglia. They found AXIS microglia occur early in development (P9), increase in number until P15, and are persistent in adulthood. A preliminary data set on the formation of satellite microglia at postnatal day 9 and day 15 shows a comparable developmental pattern (personal communication M. Matyash), thus confirming the findings on AXIS microglia (data not shown).

To better understand the functional role of this interaction, it may also be plausible to study if structural proteins, cell adhesion molecules such as cadherins, and anchoring cytoskeleton or juxtaposed organelles determine the contact site. This could indicate the regions of enhanced adhesive potential (Liu et al., 2010), signaling events, or homeostatic function.

Microglia establish direct contacts with different compartments of a neuron, and these microglia–neuron interactions probably serve different functions depending on the compartment-specific neuronal functions and signaling pathways (Cserep et al., 2021). Satellite microglia, due to their physical membrane interaction, have been suggested to provide metabolic support to highly active neurons, or to be involved in synaptic remodeling (Baalman et al., 2015; Schafer & Stevens, 2015; Streit, 2005). Recently, a specialized morpho-functional interaction site between neuronal somata and microglial cell processes has been described (Cserep et al., 2020); these tight membrane–membrane associations are equipped with a specialized nanoarchitecture optimized for purinergic signaling and may potentially monitor neuronal functions. Whether a similar cross talk via direct membrane interaction occurs at the contact area between satellite microglia and its specific partner neuron remains to be shown. Likely, the communication mechanisms are as heterogeneous as the interacting cellular partners and may be governed by the neurotransmitter systems expressed by the given partner neurons.

Microglia express a plethora of neurotransmitter receptors (Pocock & Kettenmann, 2007) and have the capacity to communicate with neurons via the receptor-coupled signaling systems. In functional electrophysiological studies of freshly isolated microglia, certain subsets of the total population respond in different proportions to serotonin, dopamine, and several other neurotransmitters or peptides (Pannell et al., 2014), suggesting microglia diversity in terms of neurotransmitter receptor expression. A preference of microglia to form satellites with a neuron of a specific transmitter type may facilitate the cross talk among the cellular partners, for instance signal a metabolic need. Regulatory signals must have a short radius of action rather than being broadly diffusible. Recent studies on transcriptional heterogeneity of microglia (Grabert et al., 2016; Masuda et al., 2019, 2020; Stevens & Schafer, 2018) do not provide a conclusive image of presence of distinct subpopulations of microglia in the normal adult mouse brain. Thus, correlating transcriptionally and morphologically distinct subtypes, including satellite microglia, is not yet possible. Further development in the field of employing a combination of imaging and transcriptional analysis, including Patch-seq or spatial single-cell transcriptomics might become instrumental for answering this broad question and allowing a better understanding of satellite microglia function.

DECLARATION OF TRANSPARENCY

The authors, reviewers and editors affirm that in accordance to the policies set by the *Journal of Neuroscience Research*, this manuscript presents an accurate and transparent account of the study being reported and that all critical details describing the methods and results are present.

ACKNOWLEDGMENTS

The authors are grateful to Nadine Scharek and Inga Krüger for excellent technical assistance. They thank the Advanced Light Microscopy facility at the Max-Delbrück-Center for Molecular Medicine in the Helmholtz Association (MDC), Berlin, Germany (https://www.mdc-berlin.de/de/technologie-plattformen), in particular Matthias Richter, for substantial technical support and assistance in this work, Nine Kompier for statistics advise, and PD Dr. Friederike Klempin for providing tissue of Tph2-eYFP transgenic mice.

CONFLICT OF INTEREST

The authors declare no conflict of interest related to this study.

AUTHOR CONTRIBUTIONS

All authors had full access to all data in the study and take responsibilities on the data integrity and accuracies of the data analysis. *Conceptualization*, H.K. and C.N. *Methodology*, O.B. and C.N.; *Investigation*, O.B. and C.N.; *Formal Analysis*, O.B. and C.N.; *Writing – Original Draft*, C.N., O.B., and H.K.; *Writing - Review & Editing*, H.K., C.N.; *Visualization*, C.N. and O.B.; *Supervision*, C.N. and H.K.; *Revisions*, C.N., O.B., and H.K.

PEER REVIEW

The peer review history for this article is available at https://publons.com/publon/10.1002/jnr.25026.

DATA AVAILABILITY STATEMENT

The data that support the findings of this study are available on request from the corresponding author and are available in the German Neuroinformatics Node's (GIN)data infrastructure at https://gin.g-node.org, reference number cnolte/Satellite_microglia.

ORCID

Helmut Kettenmann https://orcid.org/0000-0001-8208-0291
Christiane Nolte https://orcid.org/0000-0001-5398-3440

REFERENCES

Baalman, K., Marin, M. A., Ho, T. S., Godoy, M., Cherian, L., Robertson, C., & Rasband, M. N. (2015). Axon initial segment-associated microglia. *Journal of Neuroscience*, *35*(5), 2283–2292. https://doi.org/10.1523/JNEUROSCI.3751-14.2015

Battefeld, A., Klooster, J., & Kole, M. H. (2016). Myelinating satellite oligodendrocytes are integrated in a glial syncytium constraining neuronal high-frequency activity. *Nature Communications*, *7*, 11298. https://doi.org/10.1038/ncomms11298

Bermejo, P. E., Jimenez, C. E., Torres, C. V., & Avendano, C. (2003). Quantitative stereological evaluation of the gracile and cuneate nuclei and their projection neurons in the rat. *Journal of Comparative Neurology*, *463*(4), 419–433. https://doi.org/10.1002/cne.10747

Cannon, J. R., & Greenamyre, J. T. (2009). NeuN is not a reliable marker of dopamine neurons in rat substantia nigra. *Neuroscience Letters*, *464*(1), 14–17. https://doi.org/10.1016/j.neulet.2009.08.023

Colonna, M., & Butovsky, O. (2017). Microglia function in the central nervous system during health and neurodegeneration. *Annual Review of Immunology*, *35*, 441–468. https://doi.org/10.1146/annurev-immunol-051116-052358

Cserep, C., Posfai, B., & Denes, A. (2021). Shaping neuronal fate: Functional heterogeneity of direct microglia-neuron interactions. *Neuron*, *109*(2), 222–240. https://doi.org/10.1016/j.neuron.2020.11.007

Cserép, C., Pósfai, B., Lénárt, N., Fekete, R., László, Z. I., Lele, Z., Orsolits, B., Molnár, G., Heindl, S., Schwarcz, A. D., Ujvári, K., Környei, Z., Tóth, K., Szabadits, E., Sperlágh, B., Baranyi, M., Csiba, L., Hortobágyi, T., Maglóczky, Z., … Dénes, Á. (2020). Microglia monitor and protect neuronal function through specialized somatic purinergic junctions. *Science*, *367*(6477), 528–537. https://doi.org/10.1126/science.aax6752

Davalos, D., Grutzendler, J., Yang, G., Kim, J. V., Zuo, Y., Jung, S., Littman, D. R., Dustin, M. L., & Gan, W. B. (2005). ATP mediates rapid microglial response to local brain injury in vivo. *Nature Neuroscience*, *8*(6), 752–758. https://doi.org/10.1038/nn1472

De Biase, L. M., Schuebel, K. E., Fusfeld, Z. H., Jair, K., Hawes, I. A., Cimbro, R., Zhang, H. Y., Liu, Q. R., Shen, H., Xi, Z. X., Goldman, D., & Bonci, A. (2017). Local cues establish and maintain region-specific phenotypes of basal ganglia microglia. *Neuron*, *95*(2), 341–356.e6. https://doi.org/10.1016/j.neuron.2017.06.020

Del Rio Hortega, P. (1919). El tercer elemento de los centros nerviosos. I La microglia en estado normal. II Intervencíon de la microglia en los procesos patológicos. III Naturaleza probable de la microglia. *Boletín de la Sociedad Española de Biología*, *9*, 69–120.

Dibaj, P., Nadrigny, F., Steffens, H., Scheller, A., Hirrlinger, J., Schomburg, E. D., Neusch, C., & Kirchhoff, F. (2010). NO mediates microglial response to acute spinal cord injury under ATP control in vivo. *Glia*, *58*(9), 1133–1144. https://doi.org/10.1002/glia.20993

Dorph-Petersen, K. A., Nyengaard, J. R., & Gundersen, H. J. (2001). Tissue shrinkage and unbiased stereological estimation of particle number and size. *Journal of Microscopy*, *204*(Pt 3), 232–246. https://doi.org/10.1046/j.1365-2818.2001.00958.x

Grabert, K., Michoel, T., Karavolos, M. H., Clohisey, S., Baillie, J. K., Stevens, M. P., Freeman, T. C., Summers, K. M., & McColl, B. (2016). Microglial brain region-dependent diversity and selective regional sensitivities to aging. *Nature Neuroscience*, *19*(3), 504–516. https://doi.org/10.1038/nn.4222

Guneykaya, D., Ivanov, A., Hernandez, D. P., Haage, V., Wojtas, B., Meyer, N., Maricos, M., Jordan, P., Buonfiglioli, A., Gielniewski, B., Ochocka, N., Cömert, C., Friedrich, C., Artiles, L. S., Kaminska, B., Mertins, P., Beule, D., Kettenmann, H., & Wolf, S. A. (2018). Transcriptional and translational differences of microglia from male and female brains. *Cell Reports*, *24*(10), 2773–2783.e6. https://doi.org/10.1016/j.celrep.2018.08.001

Gusel'nikova, V. V., & Korzhevskiy, D. E. (2015). NeuN as a neuronal nuclear antigen and neuron differentiation marker. *Acta Naturae*, *7*(2), 42–47.

Hume, D. A., Perry, V. H., & Gordon, S. (1983). Immunohistochemical localization of a macrophage-specific antigen in developing mouse retina: Phagocytosis of dying neurons and differentiation of microglial cells to form a regular array in the plexiform layers. *Journal of Cell Biology*, *97*(1), 253–257. https://doi.org/10.1083/jcb.97.1.253

Kapoor, K., Bhandare, A. M., Mohammed, S., Farnham, M. M., & Pilowsky, P. M. (2016). Microglial number is related to the number of tyrosine hydroxylase neurons in SHR and normotensive rats. *Autonomic Neuroscience*, *198*, 10–18. https://doi.org/10.1016/j.autneu.2016.05.005

Karlstetter, M., Ebert, S., & Langmann, T. (2010). Microglia in the healthy and degenerating retina: Insights from novel mouse models. *Immunobiology*, *215*(9–10), 685–691. https://doi.org/10.1016/j.imbio.2010.05.010

Kaur, C., Dheen, S. T., & Ling, E. A. (2007). From blood to brain: Amoeboid microglial cell, a nascent macrophage and its functions in developing brain. *Acta Pharmacologica Sinica*, *28*(8), 1087–1096. https://doi.org/10.1111/j.1745-7254.2007.00625.x

Keller, D., Ero, C., & Markram, H. (2018). Cell densities in the mouse brain: A systematic review. *Frontiers in Neuroanatomy*, *12*, 83. https://doi.org/10.3389/fnana.2018.00083

Kettenmann, H., Hanisch, U. K., Noda, M., & Verkhratsky, A. (2011). Physiology of microglia. *Physiological Reviews*, *91*(2), 461–553. https://doi.org/10.1152/physrev.00011.2010

Lawson, L. J., Perry, V. H., Dri, P., & Gordon, S. (1990). Heterogeneity in the distribution and morphology of microglia in the normal adult mouse brain. *Neuroscience*, *39*(1), 151–170. https://doi.org/10.1016/0306-4522(90)90229-w

Lee, J. E., Liang, K. J., Fariss, R. N., & Wong, W. T. (2008). Ex vivo dynamic imaging of retinal microglia using time-lapse confocal microscopy. *Investigative Ophthalmology & Visual Science*, *49*(9), 4169–4176. https://doi.org/10.1167/iovs.08-2076

Liu, Z., Tan, J. L., Cohen, D. M., Yang, M. T., Sniadecki, N. J., Ruiz, S. A., Nelson, C. M., & Chen, C. S. (2010). Mechanical tugging force regulates the size of cell-cell junctions. *Proceedings of the National Academy of Sciences of the United States of America*, *107*(22), 9944–9949. https://doi.org/10.1073/pnas.0914547107

Madisen, L., Zwingman, T. A., Sunkin, S. M., Oh, S. W., Zariwala, H. A., Gu, H., Ng, L. L., Palmiter, R. D., Hawrylycz, M. J., Jones, A. R., Lein, E. S., & Zeng, H. (2010). A robust and high-throughput Cre reporting and characterization system for the whole mouse brain. *Nature Neuroscience*, *13*(1), 133–140. https://doi.org/10.1038/nn.2467

Masuda, T., Sankowski, R., Staszewski, O., Bottcher, C., Amann, L., Sagar, Scheiwe, W., Nessler, S., Kunz, P., van Loo, G., Coenen, V. A., Reinacher, P. C., Michel, A., Sure, U., Gold, R., Grün, D., Priller, J., Stadelmann, C., & Prinz, M. (2019). Spatial and temporal heterogeneity of mouse and human microglia at single-cell resolution. *Nature*, *566*(7744), 388–392. https://doi.org/10.1038/s41586-019-0924-x

Masuda, T., Sankowski, R., Staszewski, O., & Prinz, M. (2020). Microglia heterogeneity in the single-cell era. *Cell Reports*, *30*(5), 1271–1281. https://doi.org/10.1016/j.celrep.2020.01.010

McEwen, B. S., & Milner, T. A. (2017). Understanding the broad influence of sex hormones and sex differences in the brain. *Journal of Neuroscience Research*, *95*(1–2), 24–39. https://doi.org/10.1002/jnr.23809

Nelson, L. H., Saulsbery, A. I., & Lenz, K. M. (2019). Small cells with big implications: Microglia and sex differences in brain development, plasticity and behavioral health. *Progress in Neurobiology*, *176*, 103–119. https://doi.org/10.1016/j.pneurobio.2018.09.002

Nimmerjahn, A., Kirchhoff, F., & Helmchen, F. (2005). Resting microglial cells are highly dynamic surveillants of brain parenchyma in vivo. *Science*, *308*(5726), 1314–1318. https://doi.org/10.1126/science.1110647

Pannell, M., Szulzewsky, F., Matyash, V., Wolf, S. A., & Kettenmann, H. (2014). The subpopulation of microglia sensitive to neurotransmitters/neurohormones is modulated by stimulation with LPS, interferon-gamma, and IL-4. *Glia*, *62*(5), 667–679. https://doi.org/10.1002/glia.22633

Paxinos, G., & Franklin, K. B. J. (2001). *The mouse brain in stereotactic coordinates*. San Diego: Academic Press.

Pocock, J. M., & Kettenmann, H. (2007). Neurotransmitter receptors on microglia. *Trends in Neurosciences*, *30*(10), 527–535. https://doi.org/10.1016/j.tins.2007.07.007

Richter, N., Wendt, S., Georgieva, P. B., Hambardzumyan, D., Nolte, C., & Kettenmann, H. (2014). Glioma-associated microglia and macrophages/monocytes display distinct electrophysiological properties and do not communicate via gap junctions. *Neuroscience Letters*, *583*, 130–135. https://doi.org/10.1016/j.neulet.2014.09.035

Sasmono, R. T., Oceandy, D., Pollard, J. W., Tong, W., Pavli, P., Wainwright, B. J., Ostrowski, M. C., Himes, S. R., & Hume, D. A. (2003). A macrophage colony-stimulating factor receptor-green fluorescent protein transgene is expressed throughout the mononuclear phagocyte system of the mouse. *Blood*, *101*(3), 1155–1163. https://doi.org/10.1182/blood-2002-02-0569

Schafer, D. P., Lehrman, E. K., Kautzman, A. G., Koyama, R., Mardinly, A. R., Yamasaki, R., Ransohoff, R. M., Greenberg, M. E., Barres, B. A., & Stevens, B. (2012). Microglia sculpt postnatal neural circuits in an activity and complement-dependent manner. *Neuron*, *74*(4), 691–705. https://doi.org/10.1016/j.neuron.2012.03.026

Schafer, D. P., & Stevens, B. (2015). Microglia function in central nervous system development and plasticity. *Cold Spring Harbor Perspectives in Biology*, *7*(10), a020545. https://doi.org/10.1101/cshperspect.a020545

Sierra, A., de Castro, F., Del Rio-Hortega, J., Rafael Iglesias-Rozas, J., Garrosa, M., & Kettenmann, H. (2016). The "big-bang" for modern glial biology: Translation and comments on Pio del Rio-Hortega 1919 series of papers on microglia. *Glia*, *64*(11), 1801–1840. https://doi.org/10.1002/glia.23046

Sierra, A., Paolicelli, R. C., & Kettenmann, H. (2019). Cien Anos de microglia: Milestones in a century of microglial research. *Trends in Neurosciences*, *42*(11), 778–792. https://doi.org/10.1016/j.tins.2019.09.004

Stevens, B., & Schafer, D. P. (2018). Roles of microglia in nervous system development, plasticity, and disease. *Developmental Neurobiology*, *78*(6), 559–560. https://doi.org/10.1002/dneu.22594

Streit, W. J. (2005). Microglia. In H. R. Kettenmann (Ed.), *Neuroglia* (Vol. *1*, 2nd ed., pp. 60–71). Oxford University Press.

Su, P., Zhang, J., Zhao, F., Aschner, M., Chen, J., & Luo, W. (2014). The interaction between microglia and neural stem/precursor cells. *Brain Research Bulletin*, *109*, 32–38. https://doi.org/10.1016/j.brainresbull.2014.09.005

Takasaki, C., Yamasaki, M., Uchigashima, M., Konno, K., Yanagawa, Y., & Watanabe, M. (2010). Cytochemical and cytological properties of perineuronal oligodendrocytes in the mouse cortex. *European Journal of Neuroscience*, *32*(8), 1326–1336. https://doi.org/10.1111/j.1460-9568.2010.07377.x

Tremblay, M. E., Stevens, B., Sierra, A., Wake, H., Bessis, A., & Nimmerjahn, A. (2011). The role of microglia in the healthy brain. *Journal of Neuroscience*, *31*(45), 16064–16069. https://doi.org/10.1523/JNEUROSCI.4158-11.2011

Wogram, E., Wendt, S., Matyash, M., Pivneva, T., Draguhn, A., & Kettenmann, H. (2016). Satellite microglia show spontaneous electrical activity that is uncorrelated with activity of the attached neuron. *European Journal of Neuroscience*, *43*(11), 1523–1534. https://doi.org/10.1111/ejn.13256

Zhao, S., Ting, J. T., Atallah, H. E., Qiu, L., Tan, J., Gloss, B., Augustine, G. J., Deisseroth, K., Luo, M., Graybiel, A. M., & Feng, G. (2011). Cell type-specific channelrhodopsin-2 transgenic mice for optogenetic dissection of neural circuitry function. *Nature Methods*, *8*(9), 745–752. https://doi.org/10.1038/nmeth.1668

Zheng, J., Ru, W., Adolacion, J. R., Spurgat, M. S., Liu, X., Yuan, S., Liang, R. X., Dong, J., Potter, A. S., Potter, S. S., Chen, K., Chen, R., Varadarajan, N., & Tang, S. J. (2021). Single-cell RNA-seq analysis reveals compartment-specific heterogeneity and plasticity of microglia. *iScience*, *24*(3), 102186. https://doi.org/10.1016/j.isci.2021.102186

SUPPORTING INFORMATION

Additional supporting information may be found in the online version of the article at the publisher's website.

FIGURE S1 Side-by-side comparison of surface rendering approach (Imaris) and cell counter plugin approach (ImageJ) to determine if both approaches detect the same contacts/satellite microglia: *Upper row* shows four randomly cropped volumes of Z-stack images from striatum with vgat tdT labeled GABAergic neurons (magenta) and Iba-1 positive microglia (green). *The second row* shows captured 3D image of rendered surfaces of all microglia (cell bodies) in those volumes. Note the rather homogeneous distribution of microglia. White arrow indicates a microglial cell that has not been detected by the surface rendering. *Row three* shows contacts between vgat+ neurons and microglia as obtained by Imaris surface function. Orange arrows indicate two contacts that were not found with ImageJ approach (bottom row). *The bottom row* shows the cell counter windows of the same volumes; cell bodies of microglia and neurons are counted and marked with coloured tags. All identified contacts are circled: white indicates contacts matching with those obtained by Imaris. Orange circles indicate satellites which were not detected in Imaris

TABLE S1 Research Resource Identifiers (RRID) and other details of the antibodies used in the study

TABLE S2 Overview showing the brain areas and the material that was analysed, *n*: number of slices and *N*: animals analysed, the neuron types, and the analysis approach to obtain quantitative data

Transparent Science Questionnaire for Authors

Supplementary Material S2

How to cite this article: Bakina, O., Kettenmann, H. & Nolte, C. (2022). Microglia form satellites with different neuronal subtypes in the adult murine central nervous system. *Journal of Neuroscience Research*, 100, 1105–1122. https://doi.org/10.1002/jnr.25026